Atomic defects in topological and correlated twisted van der Waals heterostructures

Jose Lado

Department of Applied Physics, Aalto University, Finland

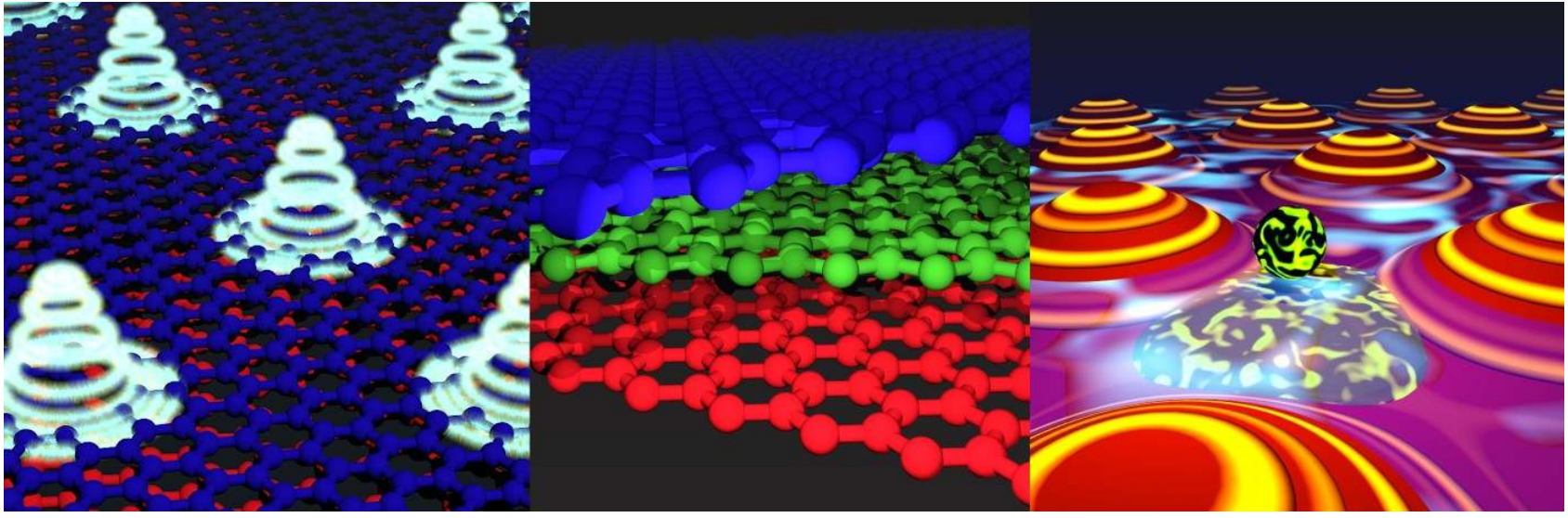

Phys. Rev. B 99, 245118 (2019)
Phys. Rev. Materials 3, 084003 (2019)

Phys. Rev. Research 2, 033357 (2020)

Phys. Rev. Materials 6, 094010 (2022)

Twistronics 2023 International Workshop on twisted bilayer graphene and beyond

January 12th 2023, Seoul, South Korea

One material, a zoo of electronic phases

Twisted bilayer graphene

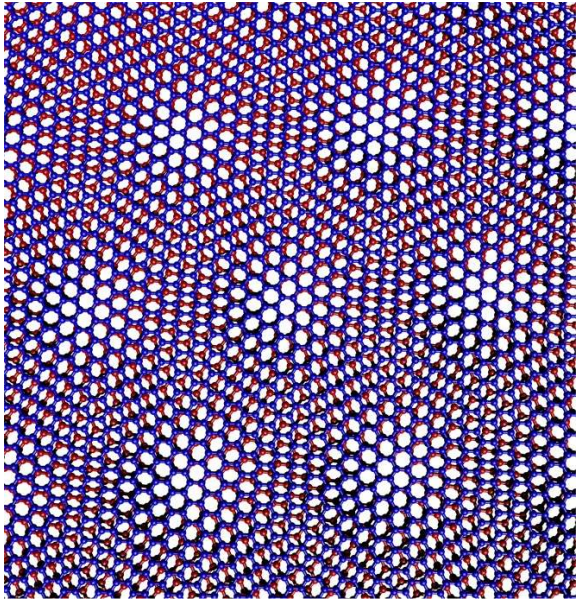

Superconductivity

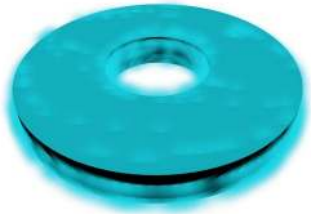

Nature 556, 43–50 (2018)

Topological networks

Nano Lett. 18, 11, 6725-6730 (2018)

Chern insulators

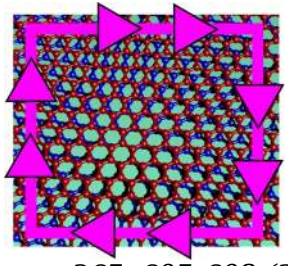

Science 365, 605-608 (2019)

Correlated insulators

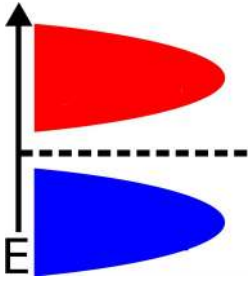

Nature 556, 80–84 (2018)

Quasicrystalline physics

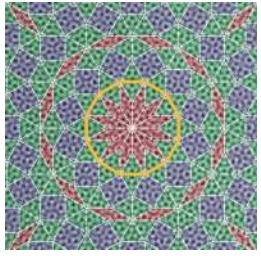

Science 361, 782-786 (2018)

Fractional Chern insulators

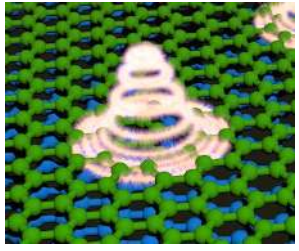

Nature 600, 439–443 (2021)

Twisted graphene multilayers provide a powerful platform for emergent phenomena

Defects in twisted van der Waals materials

Two length scales in moire systems

The original atomic scale

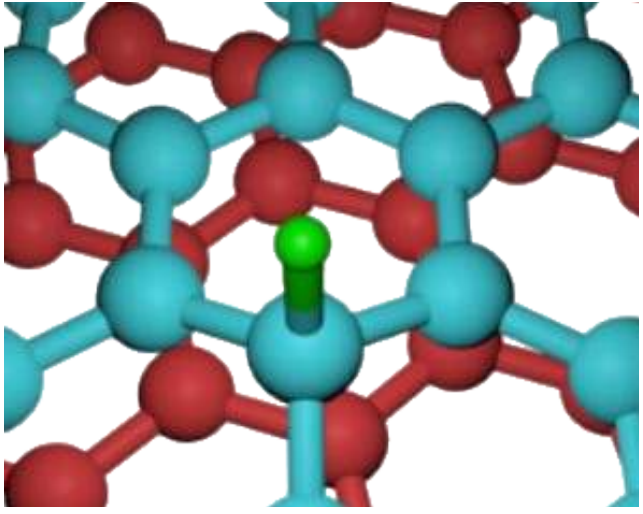

The emergent moire scale

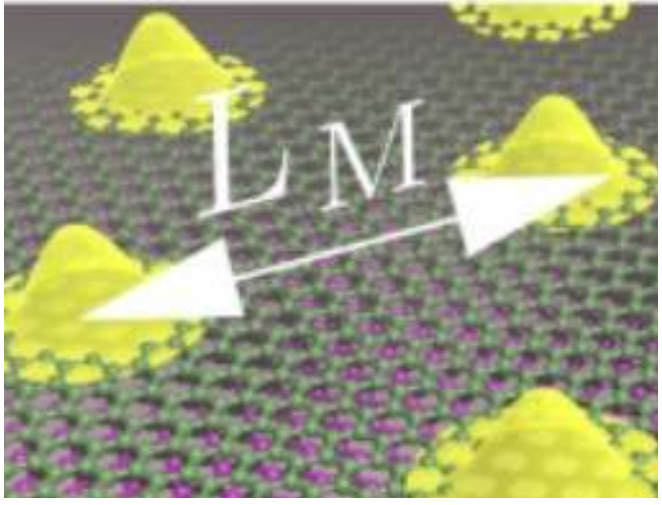

The coexistence of these two different scales is unique to moire systems

How do atomic impurities impact the physics emerging from much bigger length scales?

Today's plan

Impurities in twisted graphene bilayers

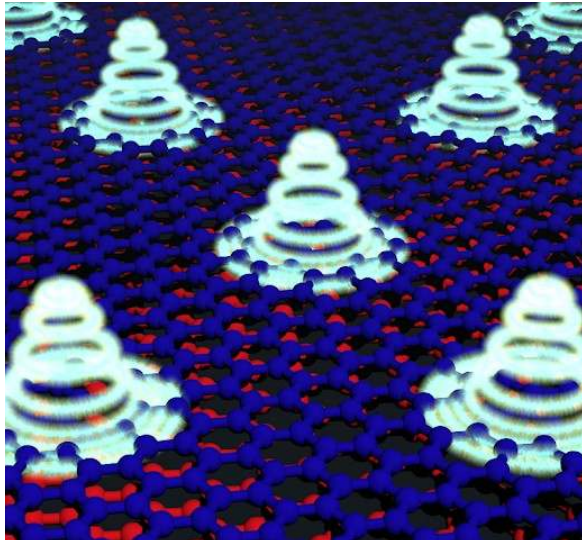

Phys. Rev. B 99, 245118 (2019)
Phys. Rev. Materials 3, 084003 (2019)

Impurities in twisted graphene trilayers

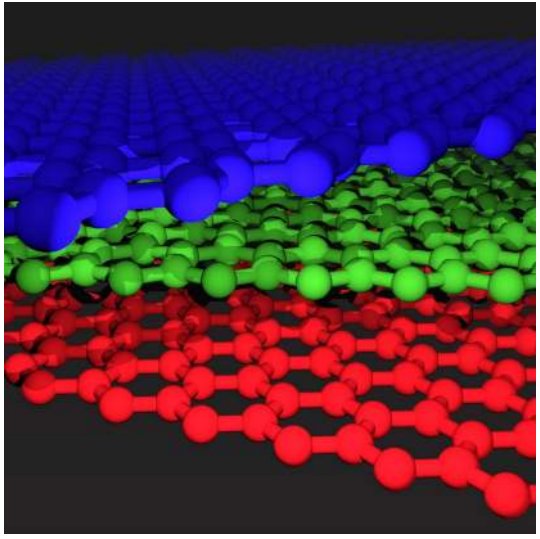

Phys. Rev. Research 2, 033357 (2020)

Impurities in twisted moire topological superconductors

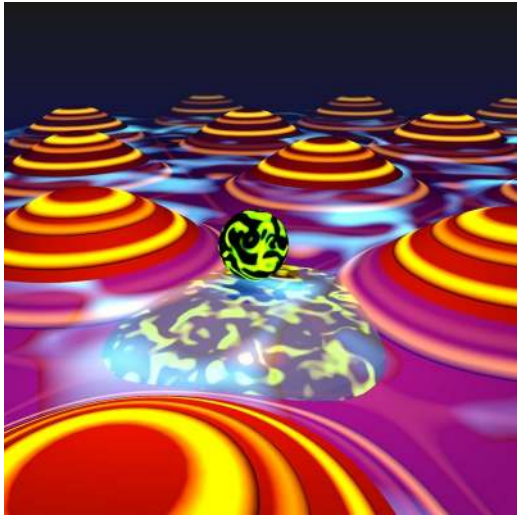

Phys. Rev. Materials 6, 094010 (2022)

Behind the scenes

Impurities in twisted graphene bilayers

Aline Ramires

Phys. Rev. B 99, 245118 (2019)

Impurities in twisted graphene trilayers

Alejandro Lopez Bezanilla

Phys. Rev. Research 2, 033357 (2020)
Phys. Rev. Materials 3, 084003 (2019)

Impurities in twisted moire topological superconductors

Maryam Khosravian

Phys. Rev. Materials 6, 094010 (2022)

Impurities in twisted bilayer graphene

Impurities in monolayer graphene

Hydrogen adsorption in graphene

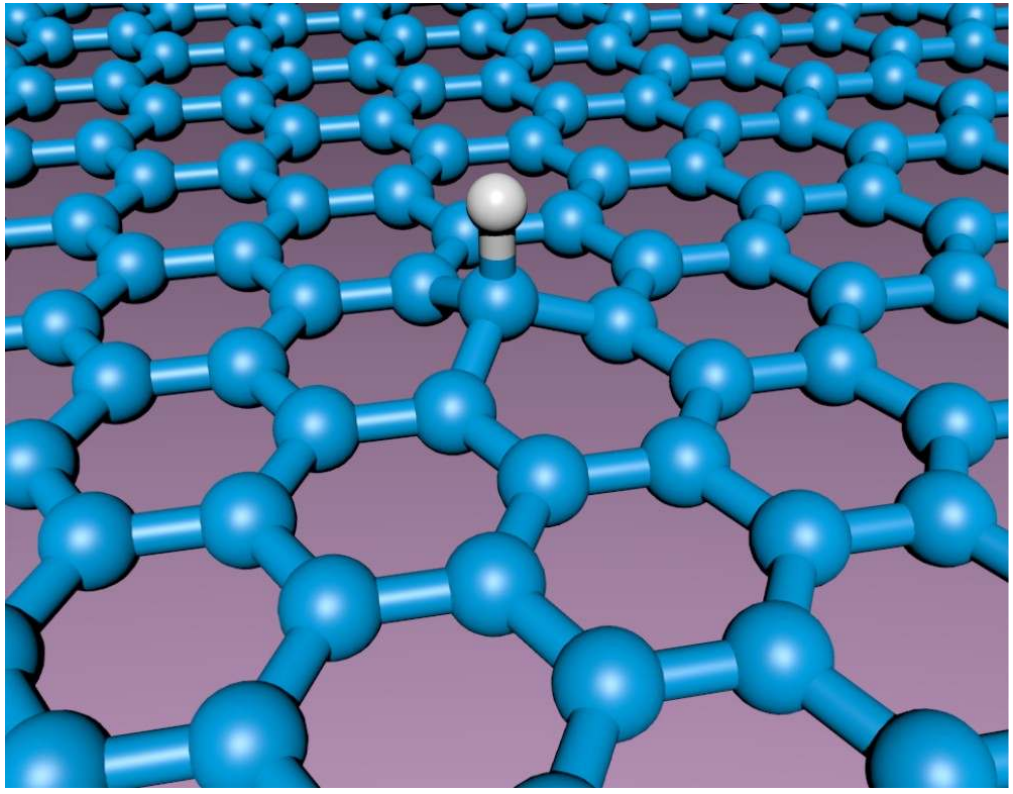

Impurities in monolayer graphene

Pristine 5x5 graphene supercell

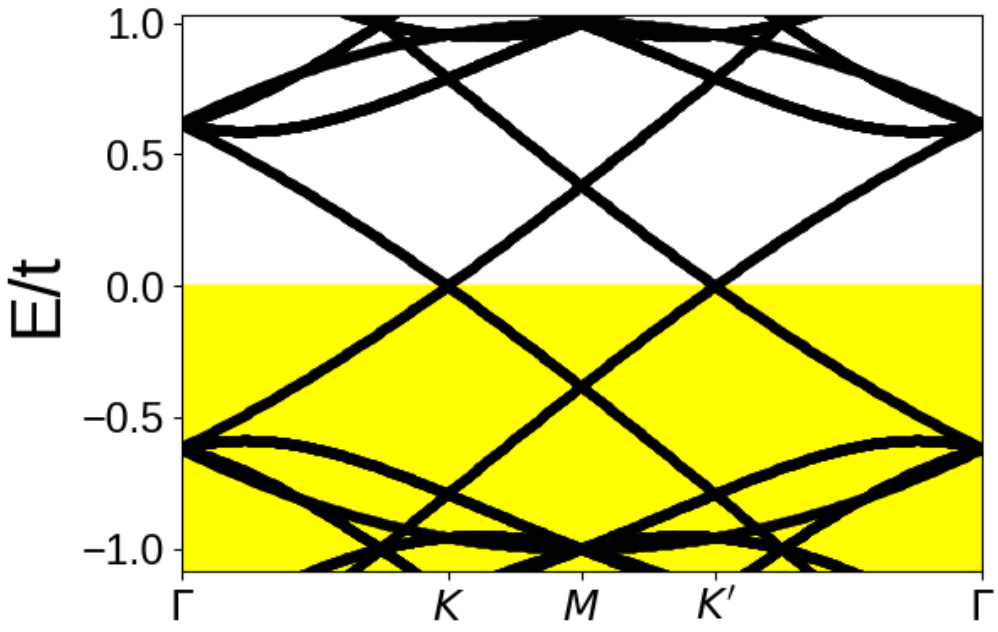

Defect in a 5x5 graphene supercell

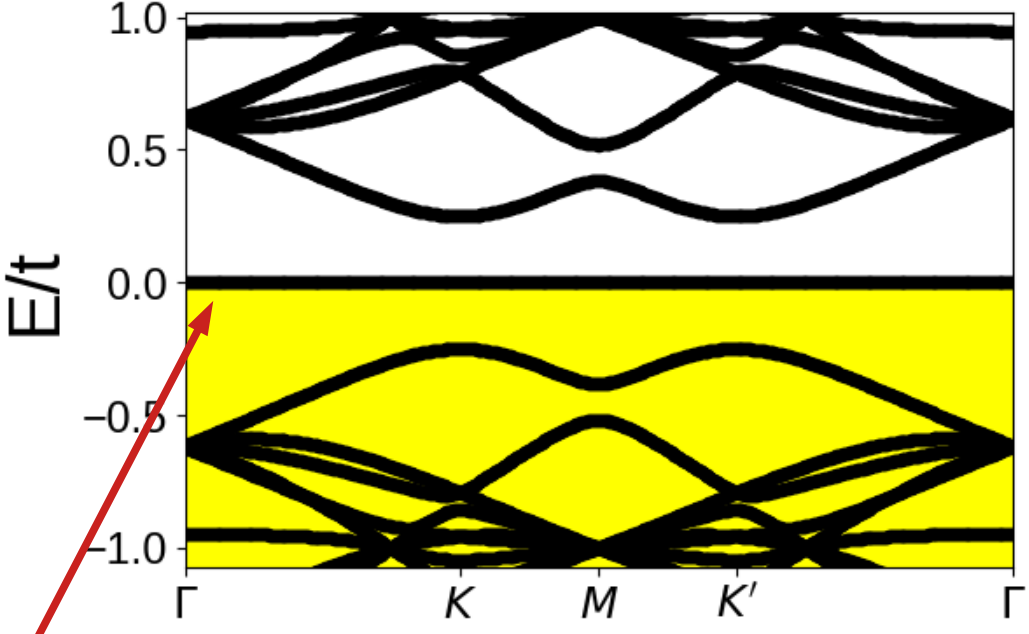

Phys. Rev. B 75, 125408 (2008)
Rep. Prog. Phys. 73 056501 (2010)

Hydrogen atoms create zero modes in graphene

Single impurity in monolayer graphene

Pristine graphene

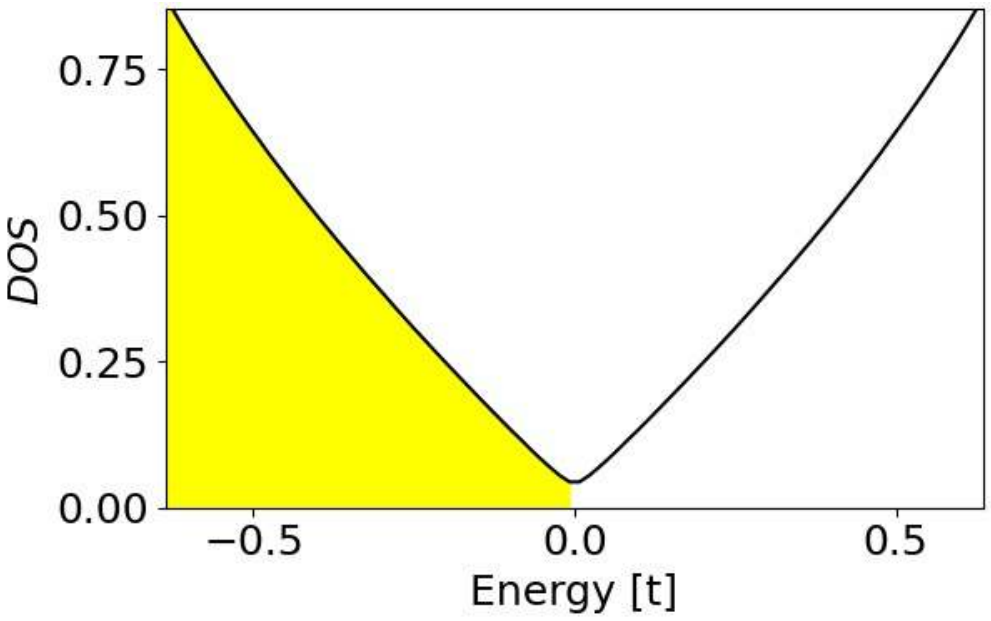

Single impurity in infinite graphene

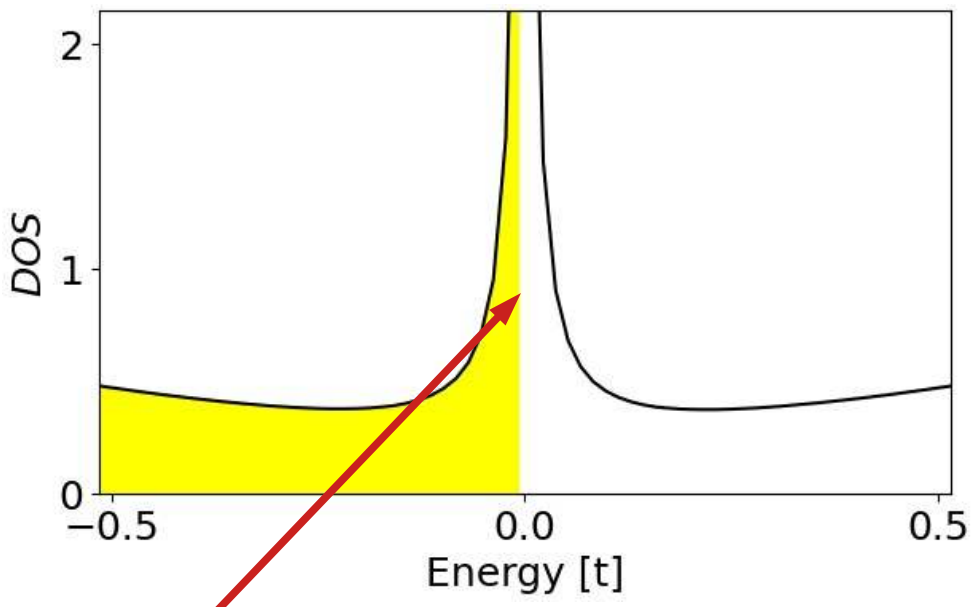

Phys. Rev. B 75, 125408 (2008)
Rep. Prog. Phys. 73 056501 (2010)

Hydrogen atoms create zero modes in graphene

Single impurity in monolayer graphene

Local density of states

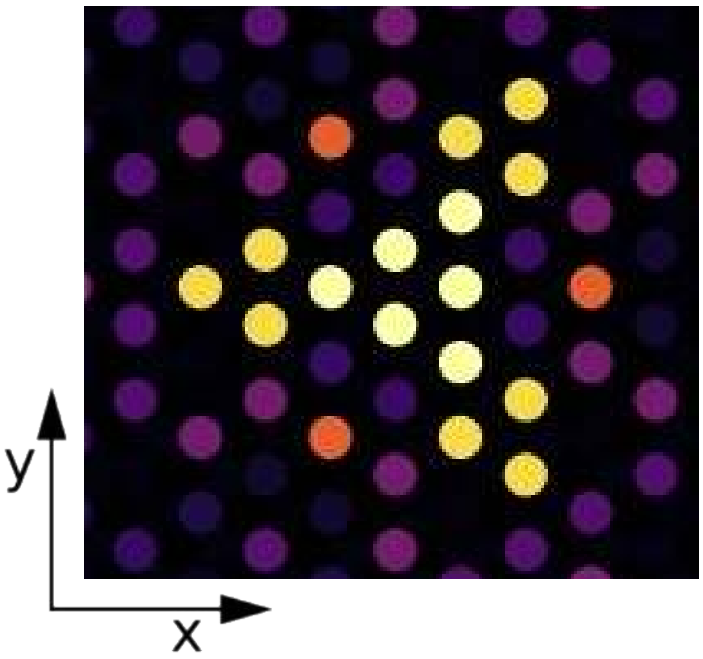

Single impurity in infinite graphene

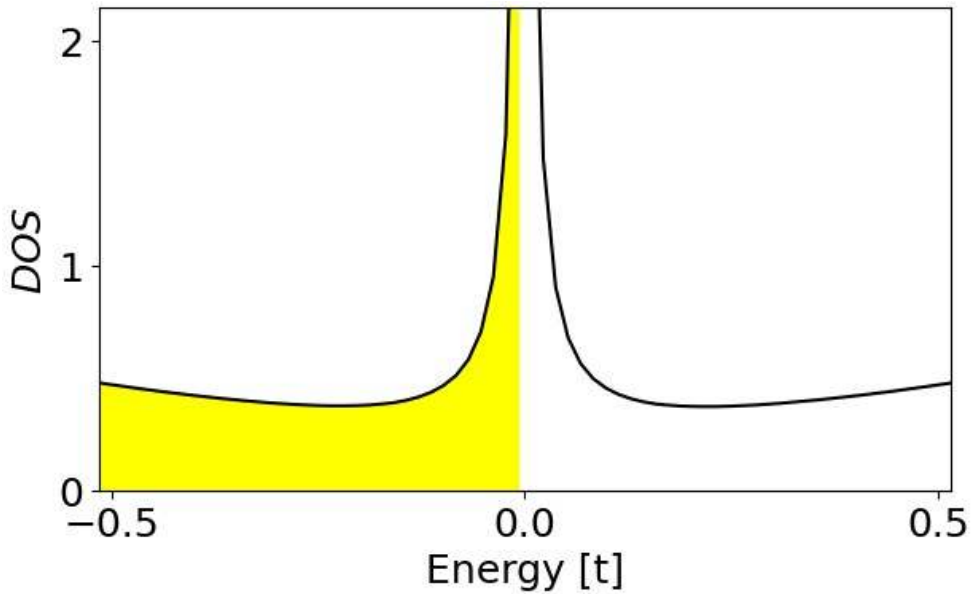

Phys. Rev. B 75, 125408 (2008)
Rep. Prog. Phys. 73 056501 (2010)

Hydrogen atoms create zero modes in graphene

Single impurity in monolayer graphene

Local density of states

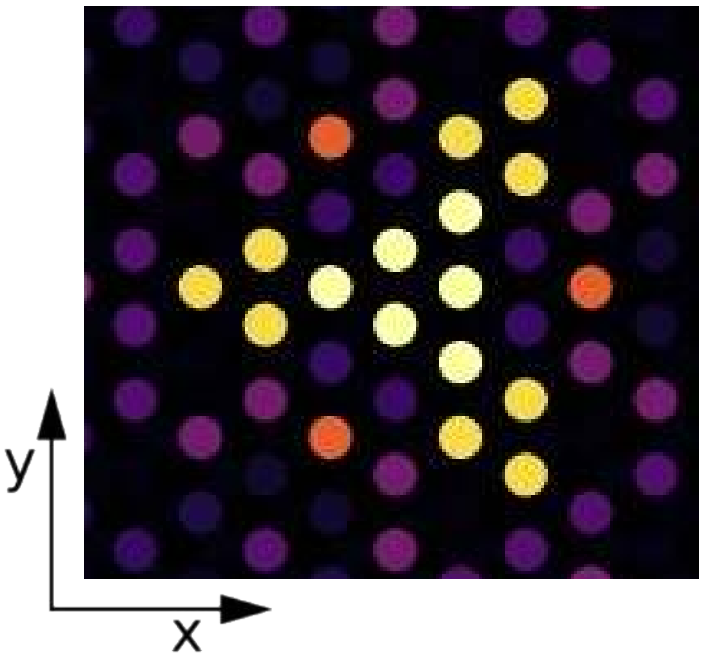

Experimental local density of states

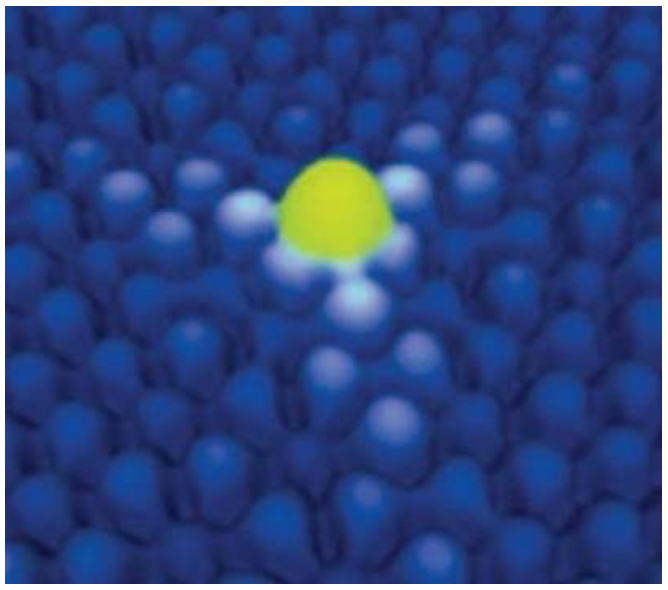

Science, 352(6284), 437-441 (2016)

Hydrogen atoms create zero modes in graphene

What can we learn from impurities

In the quantum Hall regime, local impurities generate real-space valley texture

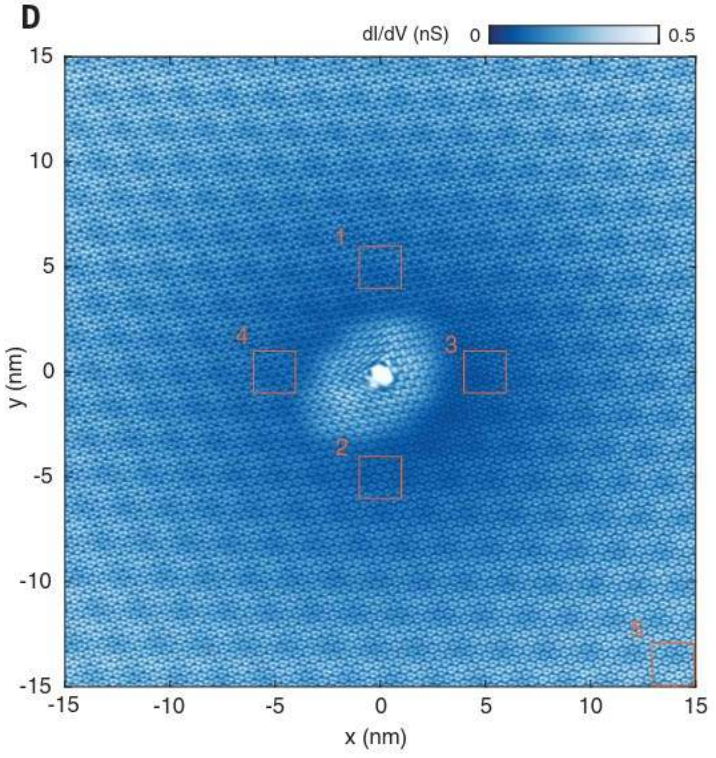

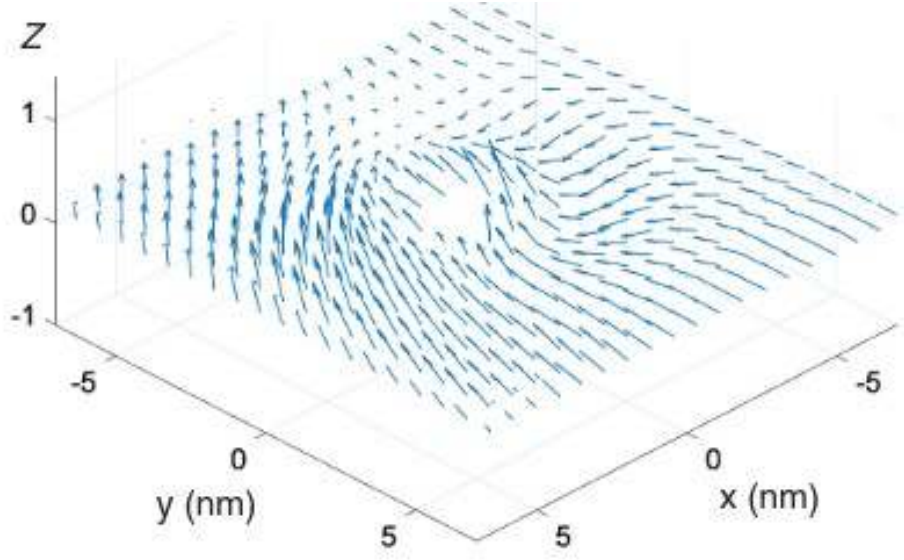

Science, 375(6578), 321-326 (2021)

Twisted graphene bilayers

Structure

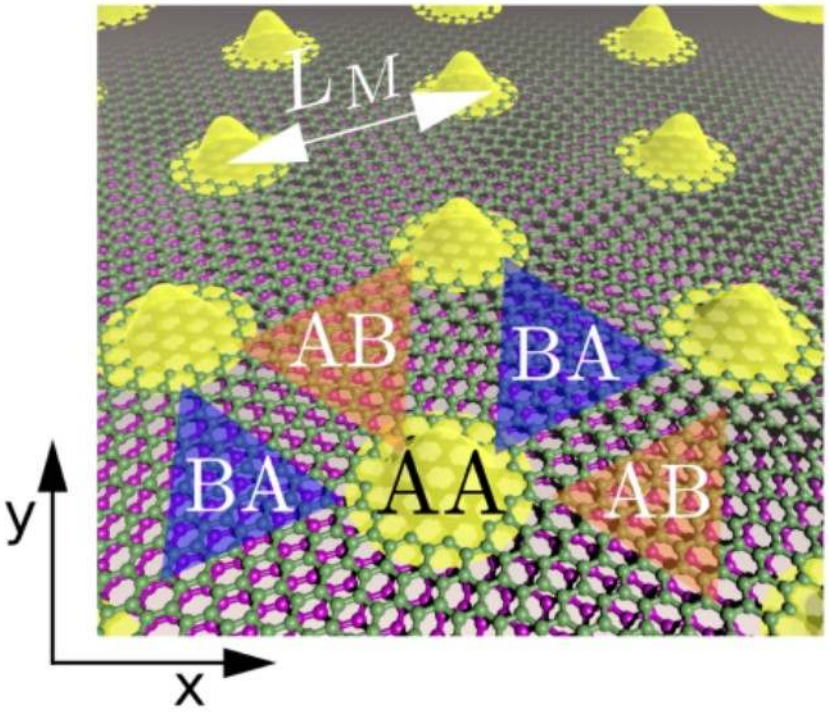

Reciprocal space

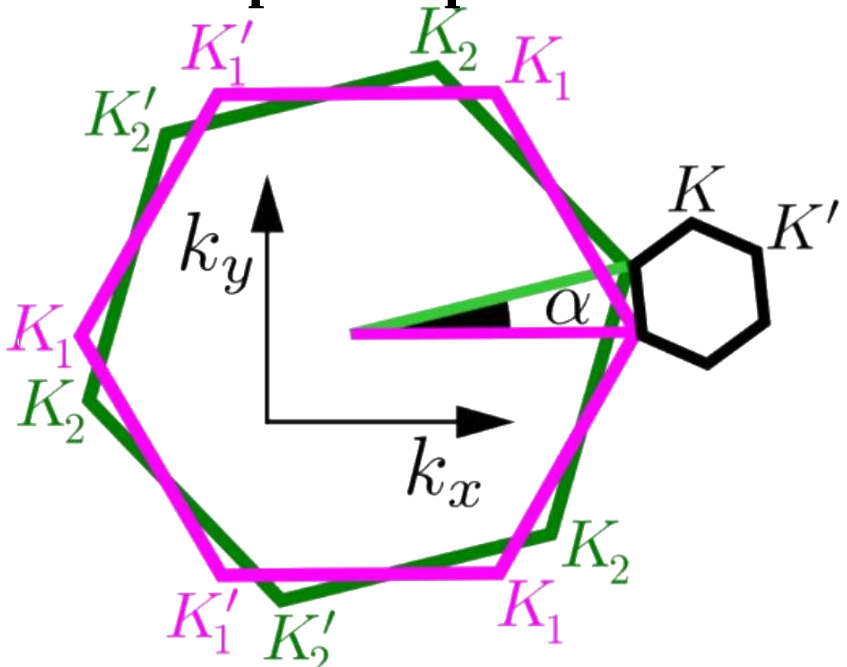

Phys. Rev. Lett. 99, 256802 (2007)
Phys. Rev. B 82, 121407(R) (2010)
PNAS 108 (30) 12233-12237 (2011)

Electronic structure of twisted bilayer

Uncoupled layers

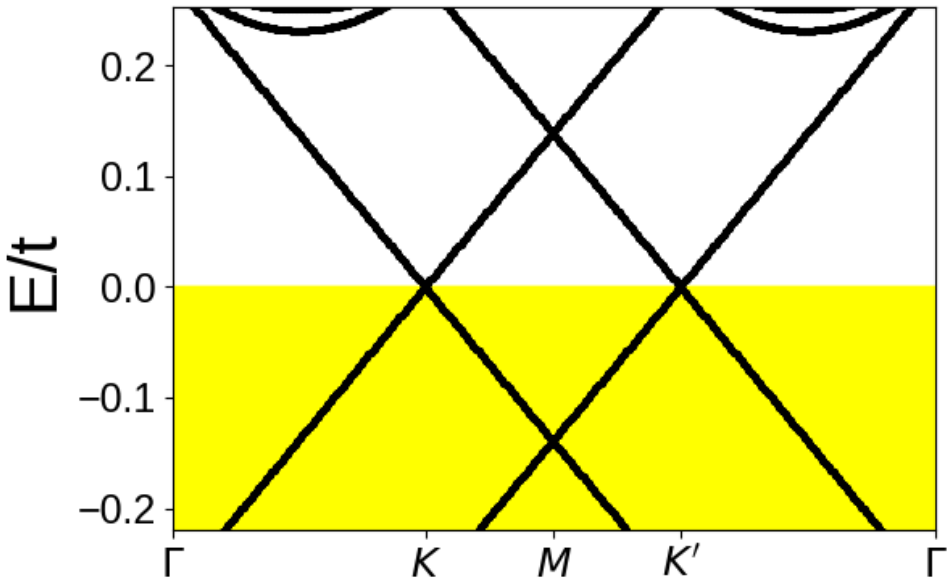

Coupled layers

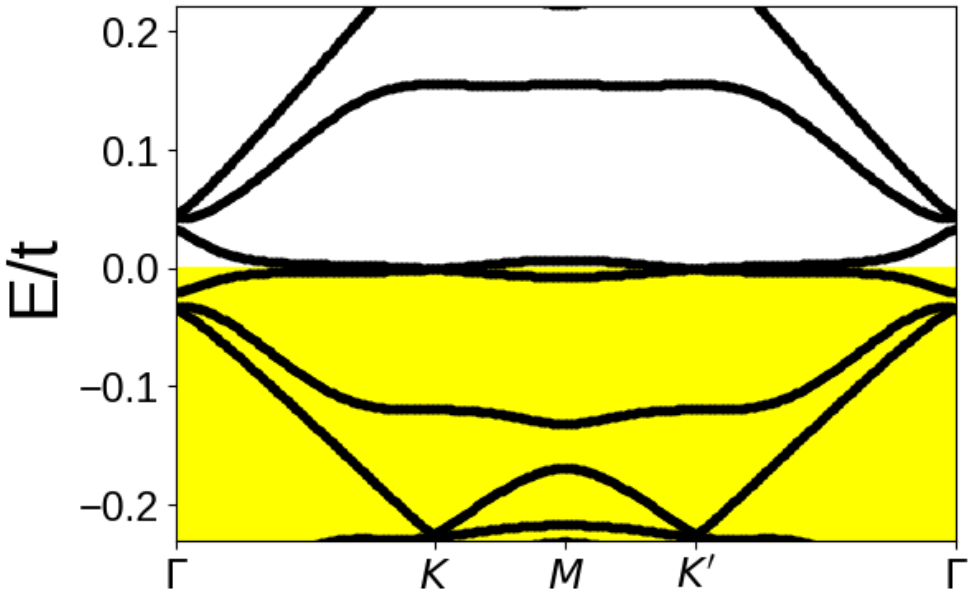

Twisted graphene bilayers feature flat bands driven by the twist

Phys. Rev. Lett. 99, 256802 (2007)
Phys. Rev. B 82, 121407(R) (2010)
PNAS 108 (30) 12233-12237 (2011)

Electronic structure of twisted bilayer

Local density of states

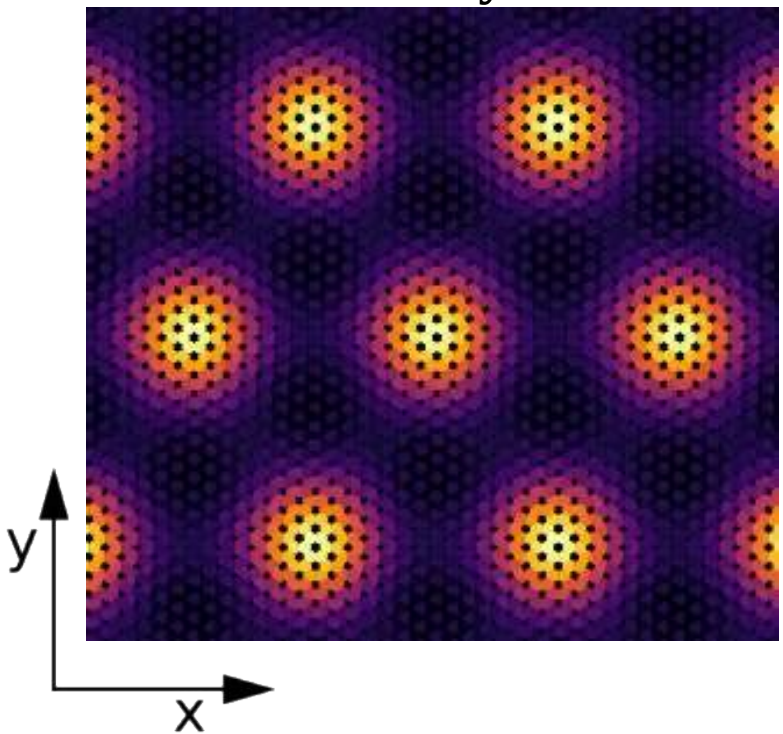

Coupled layers

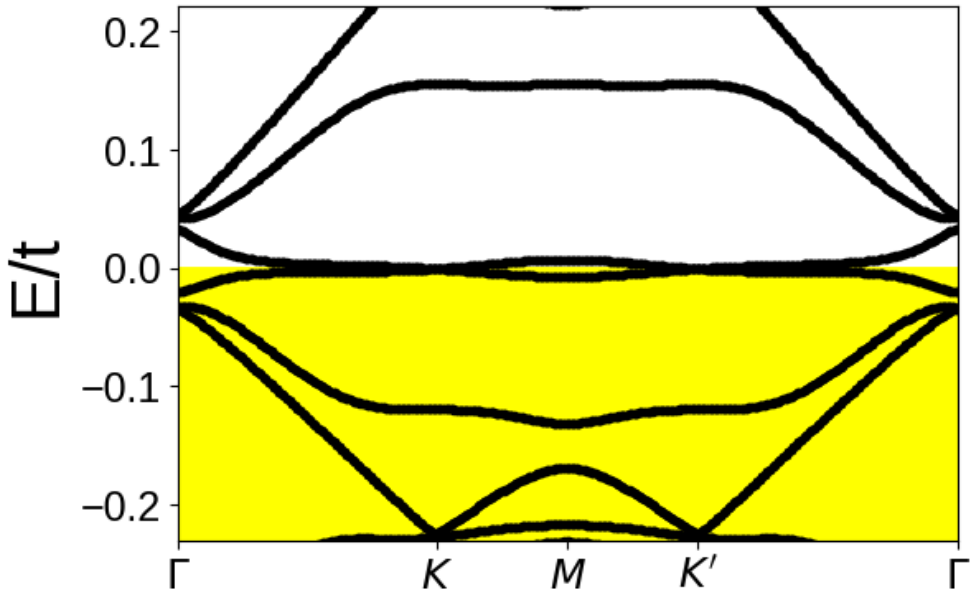

How do these moire localized modes interact with local impurities?

Phys. Rev. Lett. 99, 256802 (2007)
Phys. Rev. B 82, 121407(R) (2010)
PNAS 108 (30) 12233-12237 (2011)

Electronic structure of twisted bilayer

Local density of states

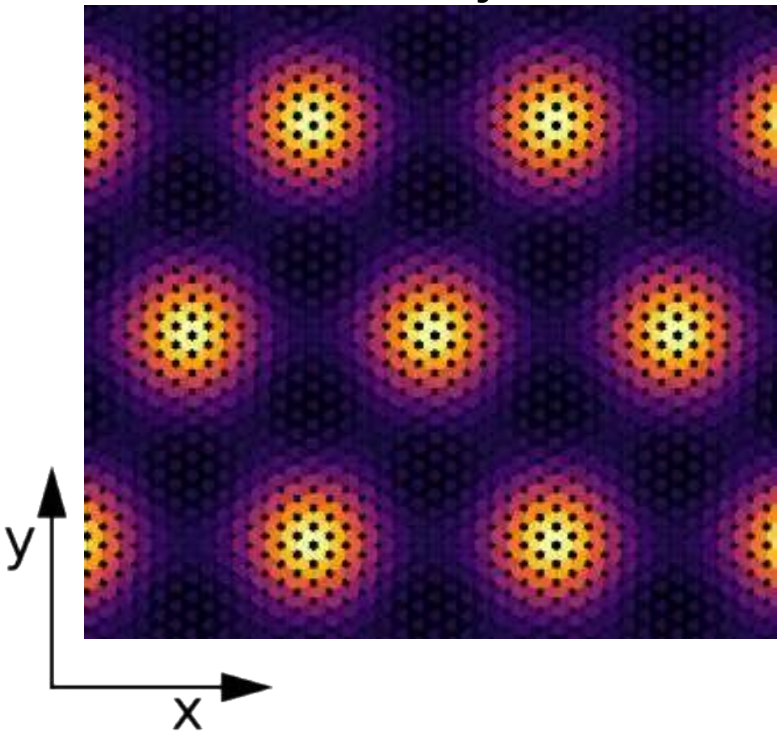

Experimental local density of states

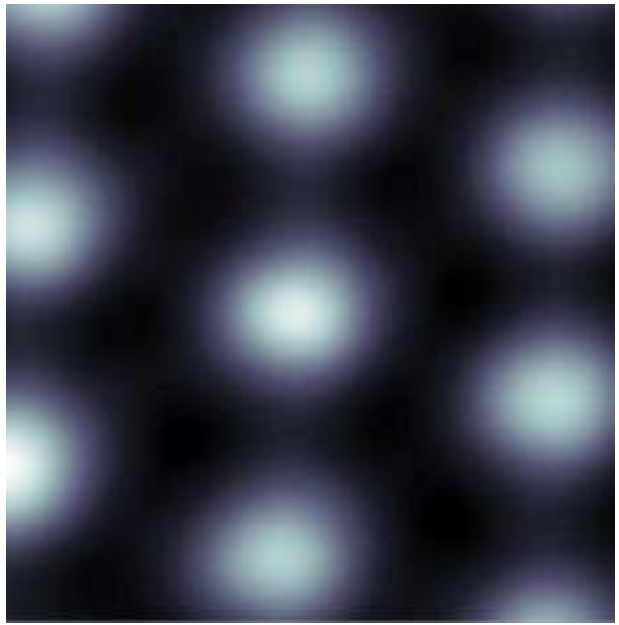

Nature Physics 6, 109–113 (2010)
Nature 572, 101–105 (2019)
Nature 572, 95–100 (2019)

How do these moire localized modes interact with local impurities?

Different impurities, different impact

Vacancy in twisted bilayer graphene

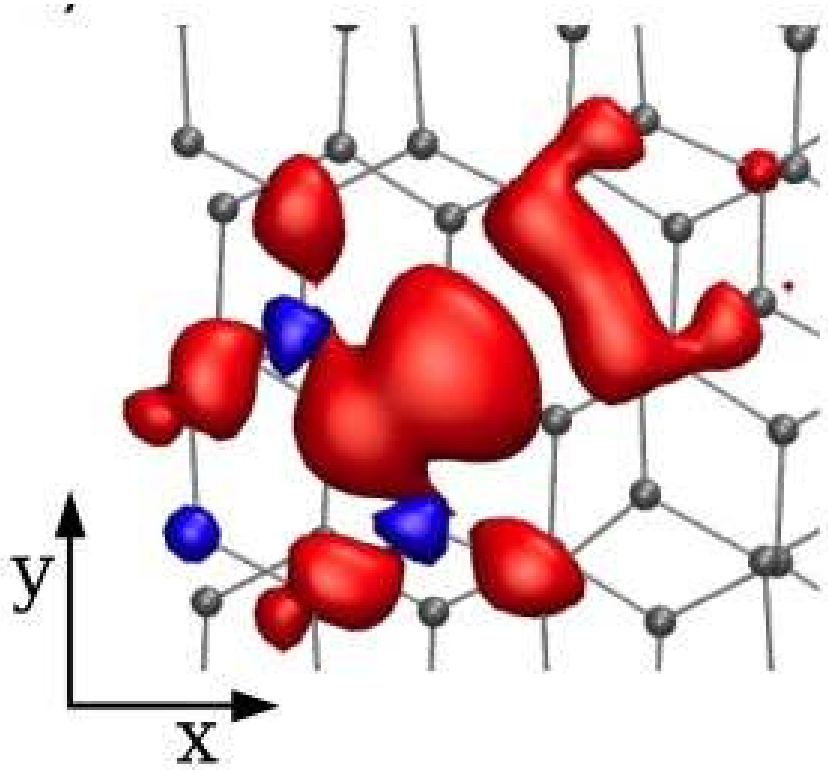

Hydrogen adsorption in twisted bilayer graphene

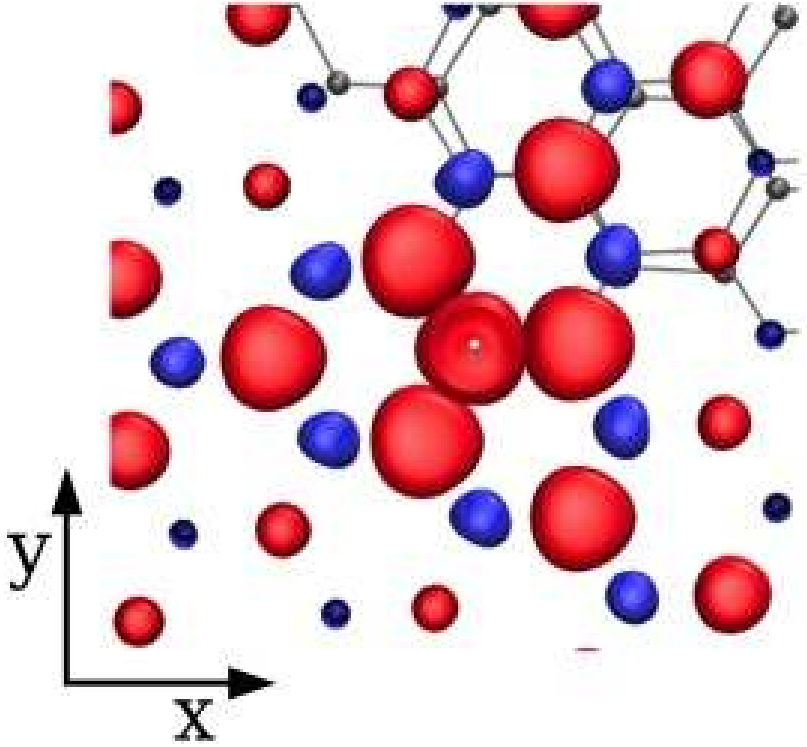

(density functional theory)

DFT for hydrogen in twisted bilayer graphene

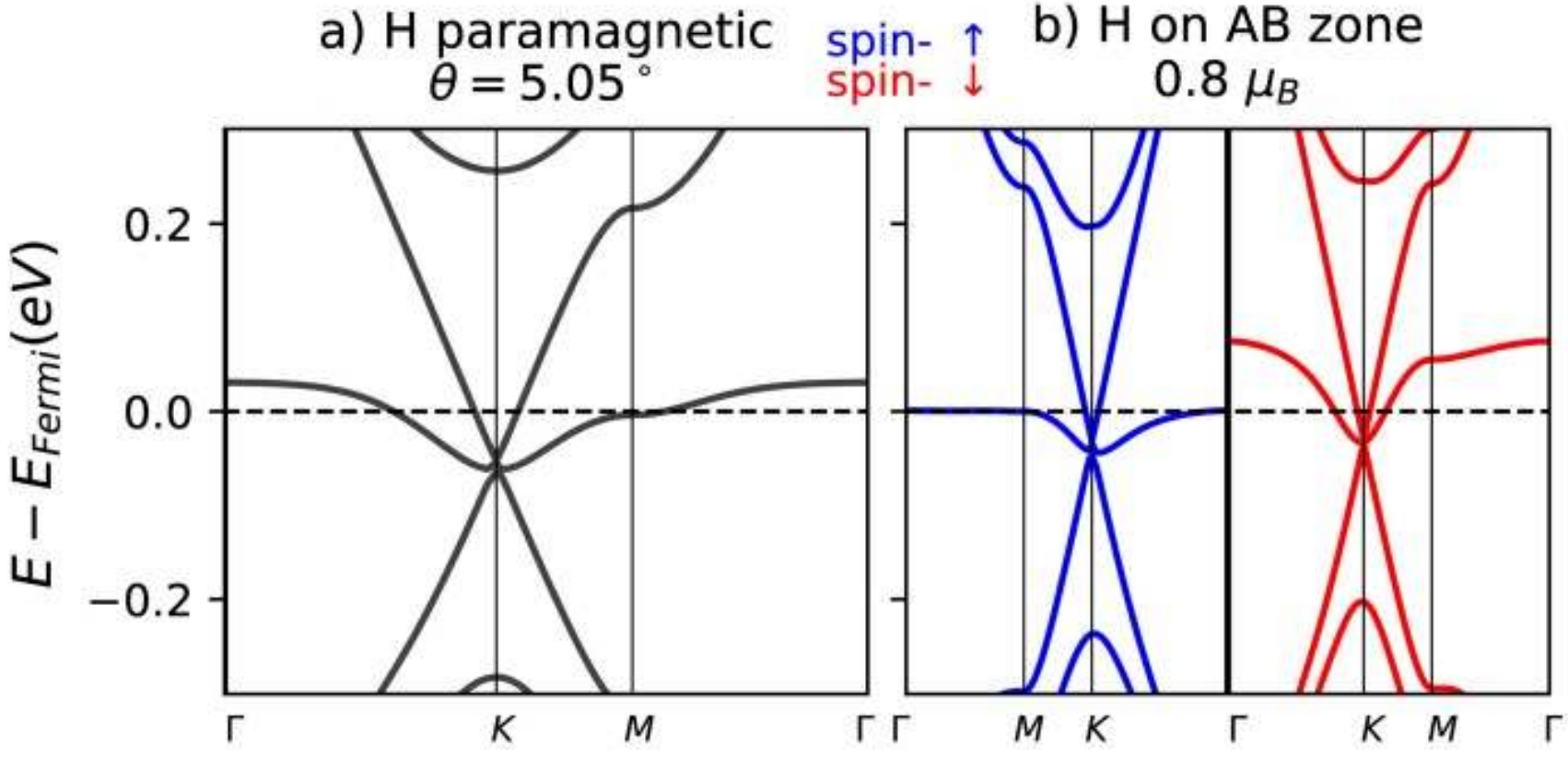

DFT for hydrogen in twisted bilayer graphene

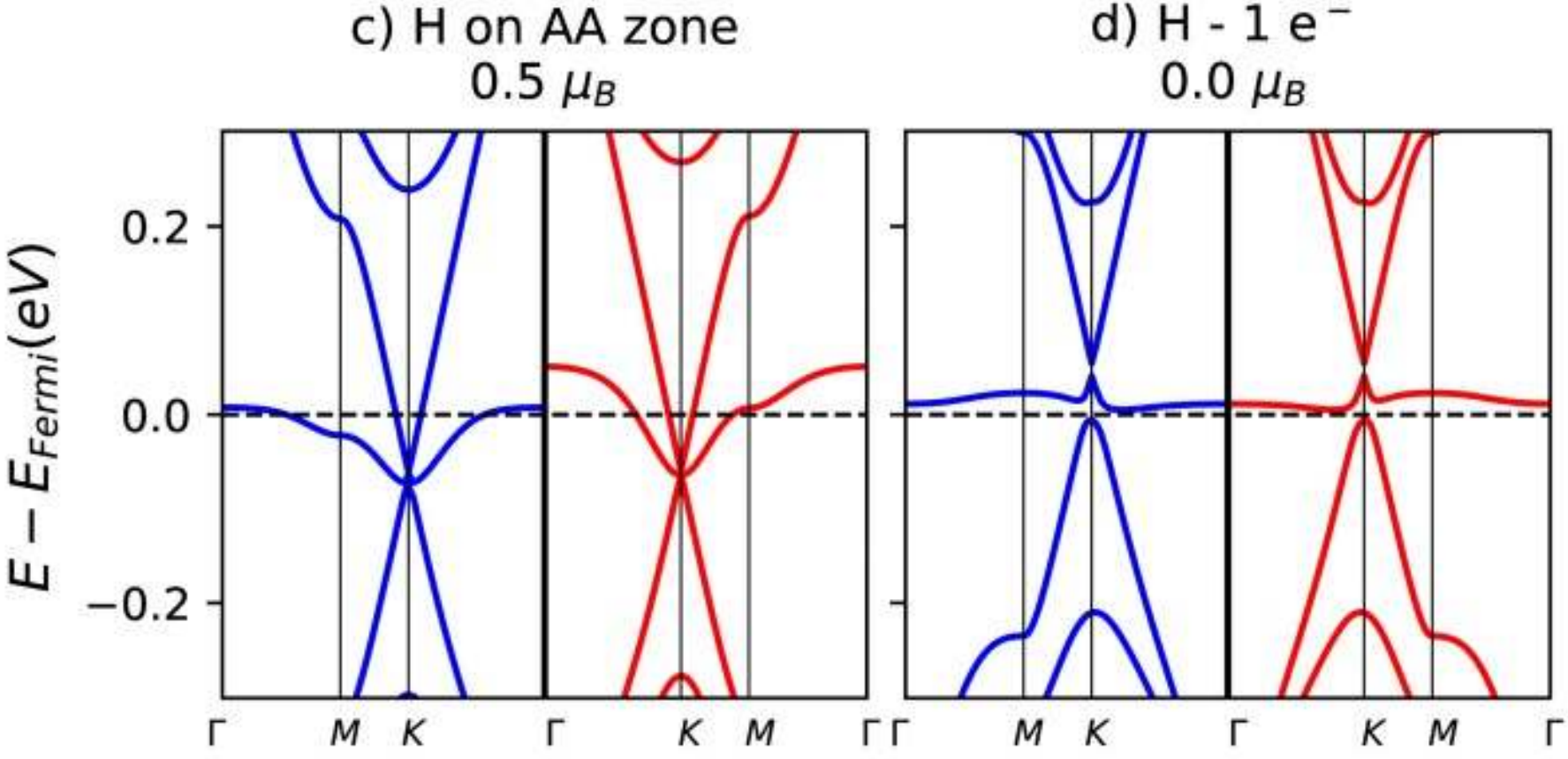

Impact of single impurities in the twisted bilayer electronic structure

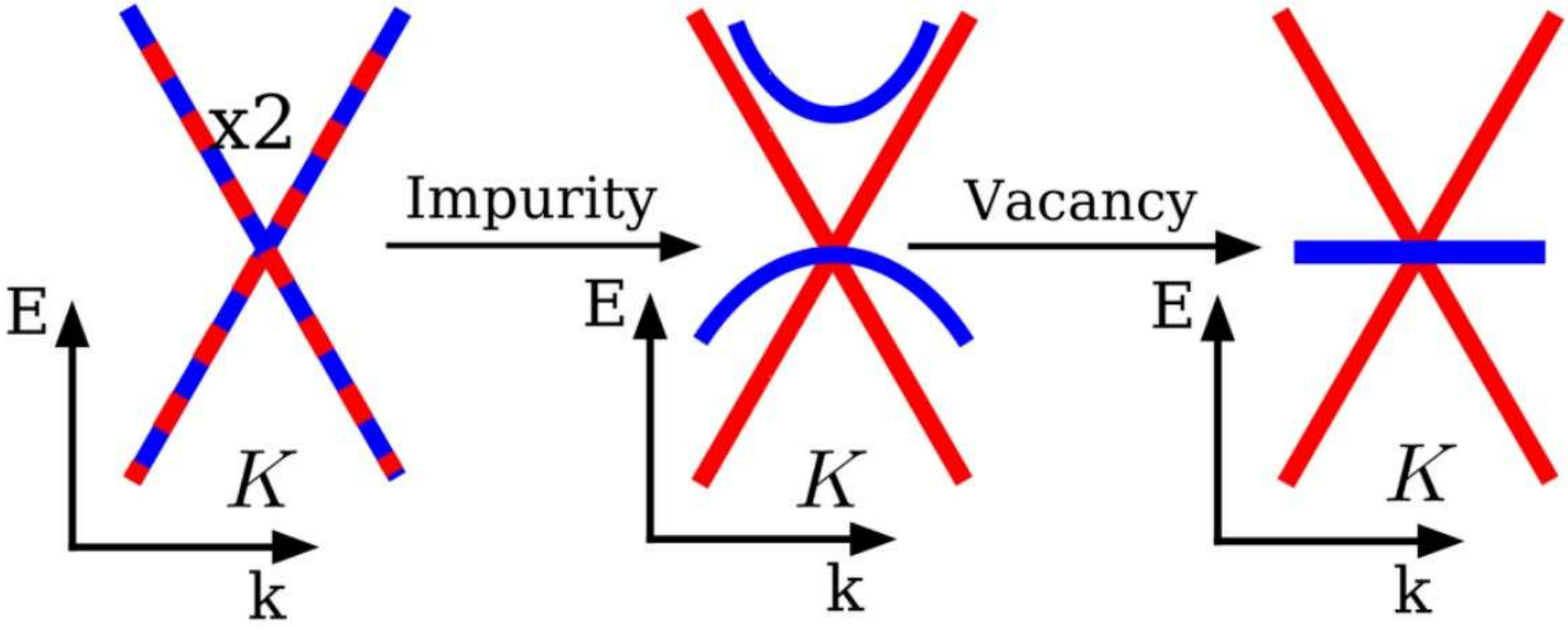

Single impurities give rise to a triple point crossing in the electronic structure

Model for impurities in twisted multilayers

Full Hamiltonian

$$\mathcal{H} = \mathcal{H}_0 + \mathcal{W}$$

Pristine twisted bilayer graphene

$$\mathcal{H}_0 = t \sum_{\langle i,j \rangle} c_i^\dagger c_j + \sum_{i,j} \bar{t}_\perp(\mathbf{r}_i, \mathbf{r}_j) c_i^\dagger c_j$$

Intra-layer hopping

Inter-layer hopping

Local impurity

$$\mathcal{W} = w c_n^\dagger c_n$$

The limit of infinite potential corresponds to removing a site

$$w \to \infty$$

The strong impurity limit

Adsorbed hydrogen in TBG

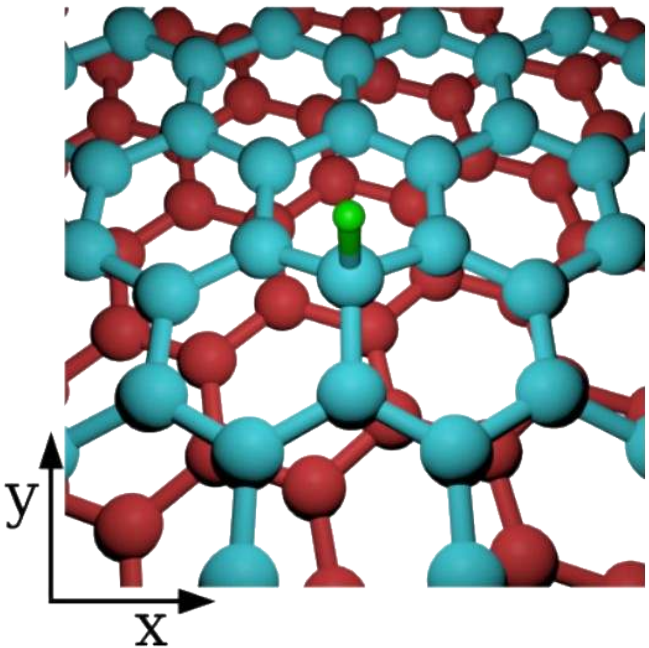

Effective tight binding model

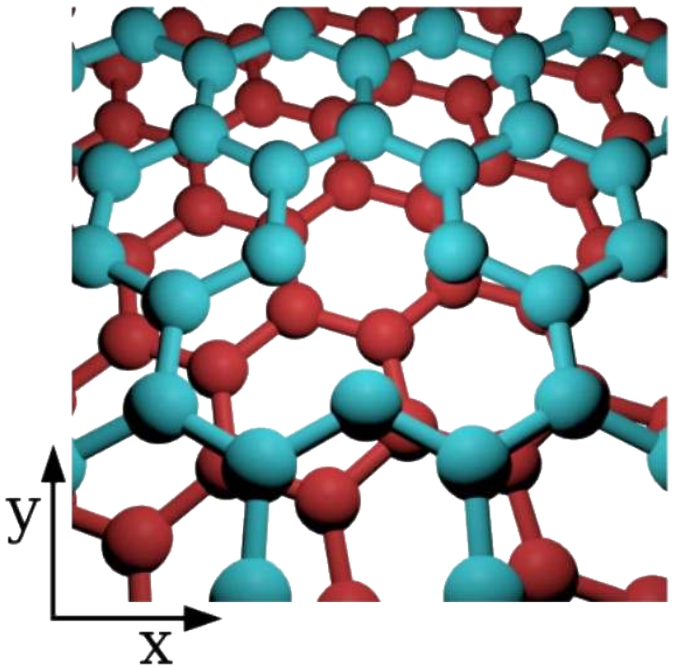

Hydrogen adsorption effectively gives rise to a vacancy in the low energy model

DFT versus tight binding

Density functional theory

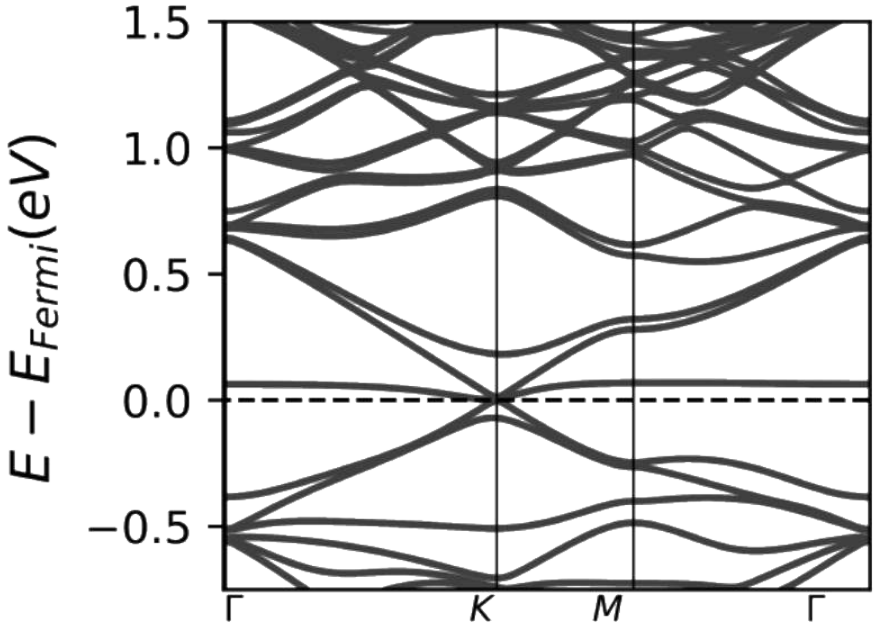

Tight binding

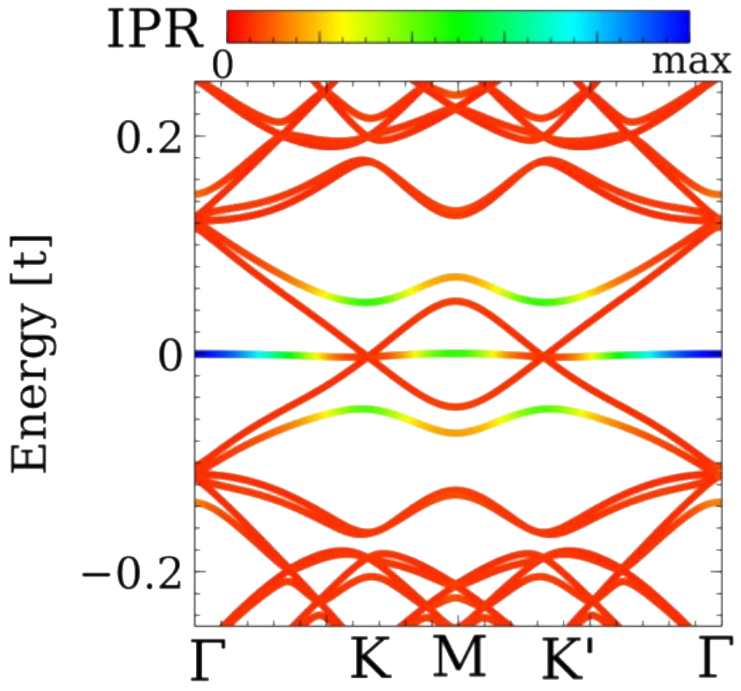

DFT and tight binding give rise to comparable electronic structures

Impact of a single weak defect

Band structure

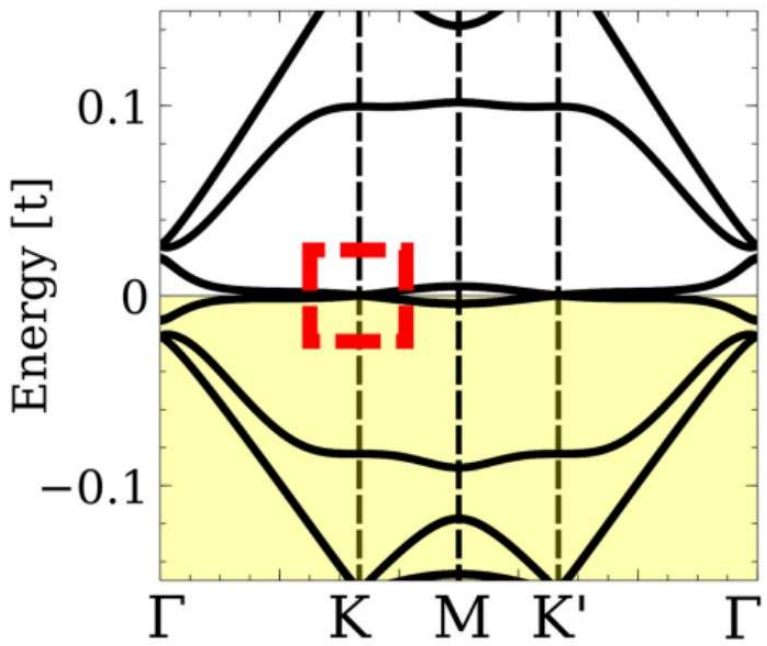

Valley expectation value

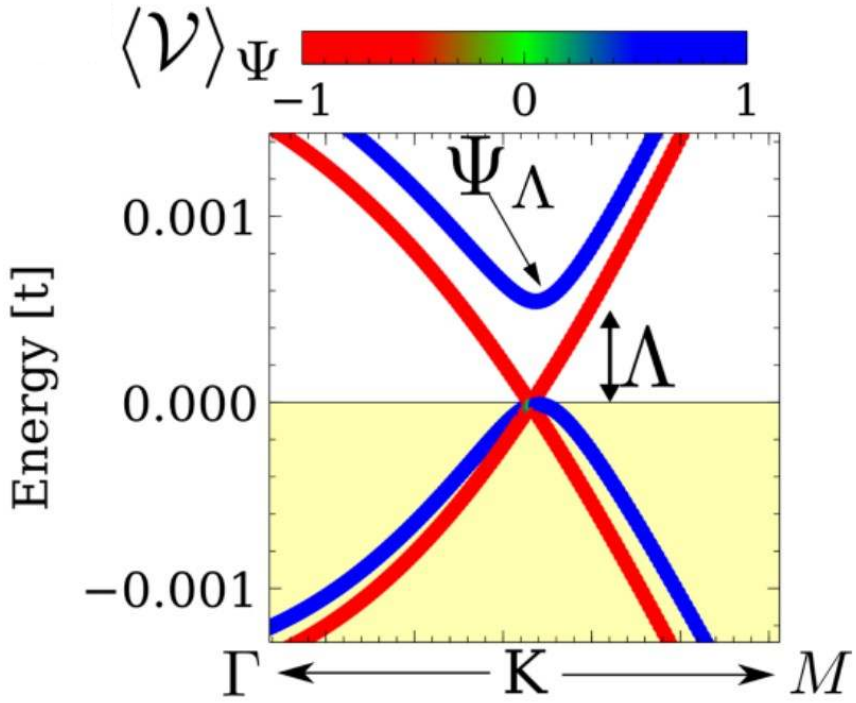

A weak impurity generates a triple band crossing at the Dirac point

Position-dependent valley mixing

Gap opening depending on the location

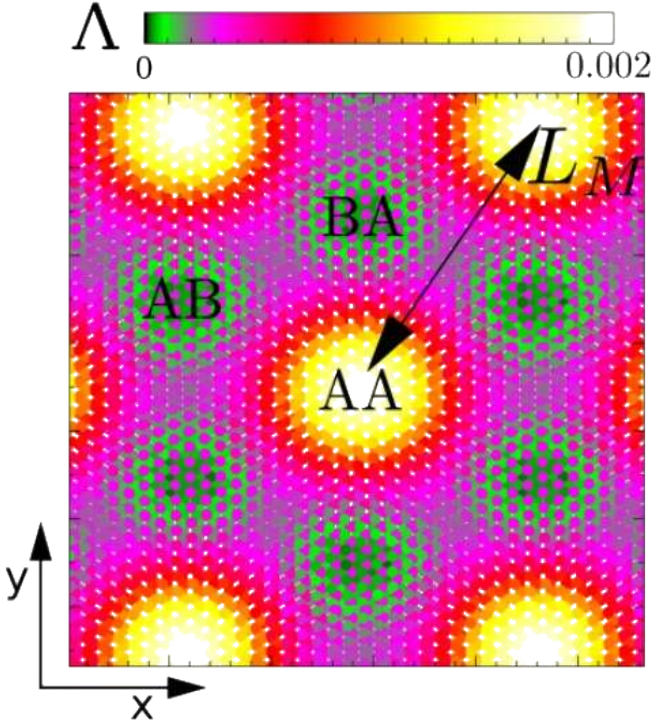

Valley polarization depending on the location

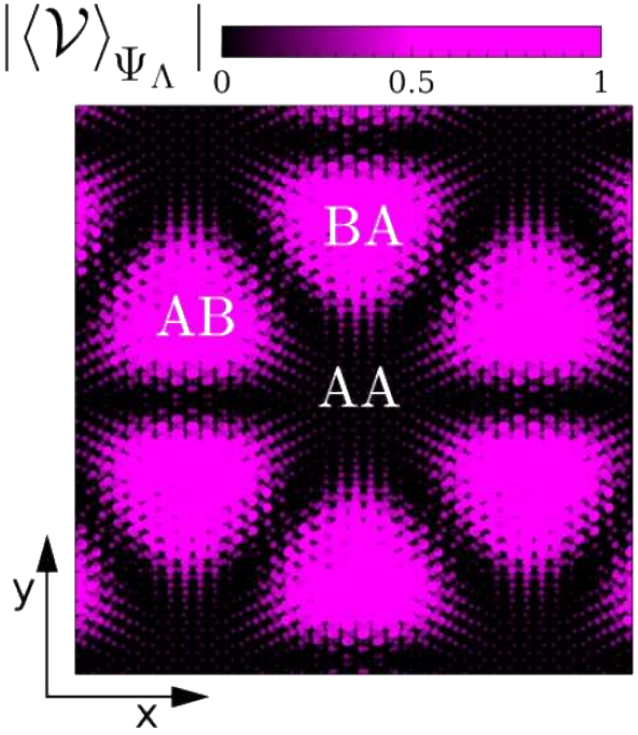

The location of the impurities determines the strength of the valley mixing

Low energy states, pristine bilayer

Band structure

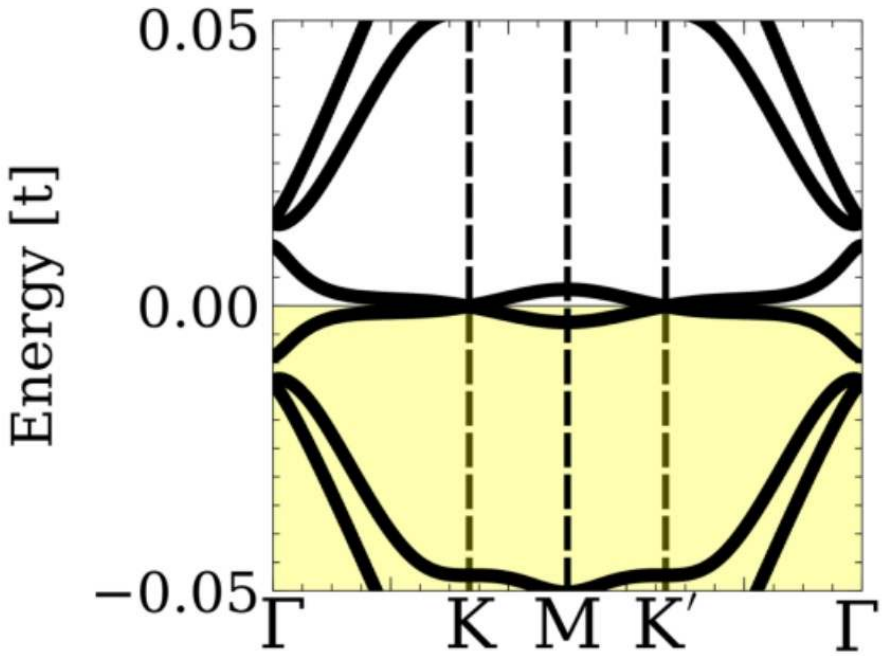

Spatial distribution of the low energy states

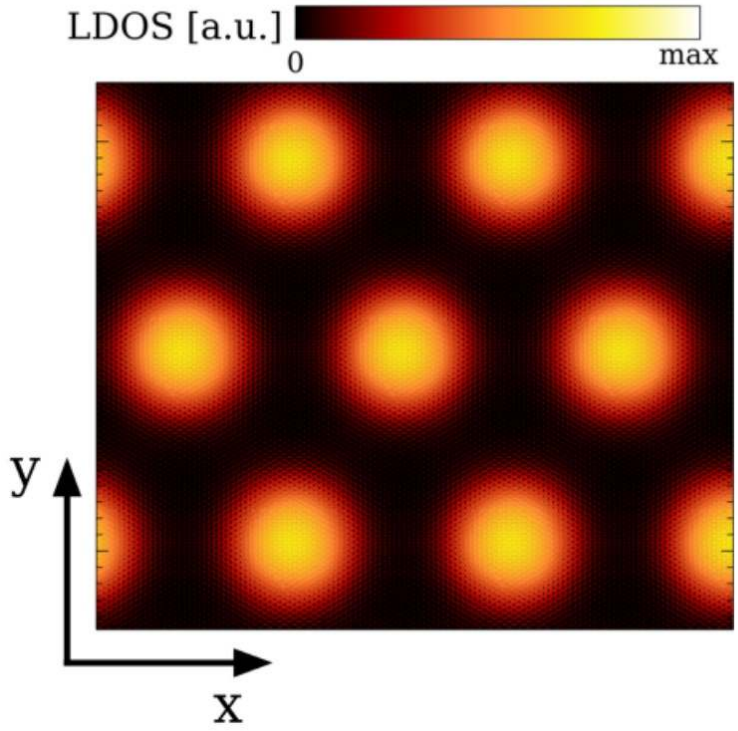

The nearly flat bands create an emergent triangular superlattice

Low energy states, strong single defect

Band structure

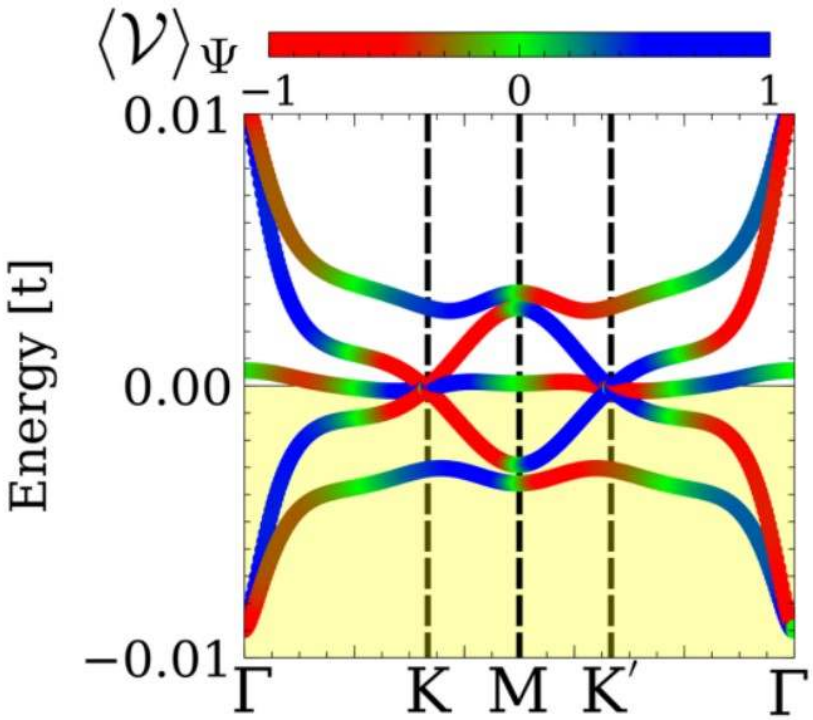

Spatial distribution of the low energy states

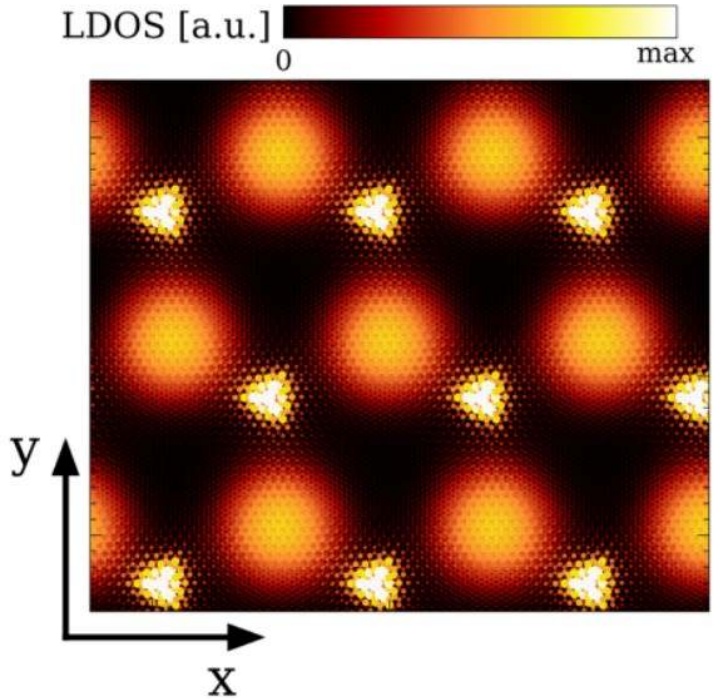

The nearly flat bands coexist with a localized vacancy state

Low energy states, strong single defect in a 4x4 supercell

Band structure

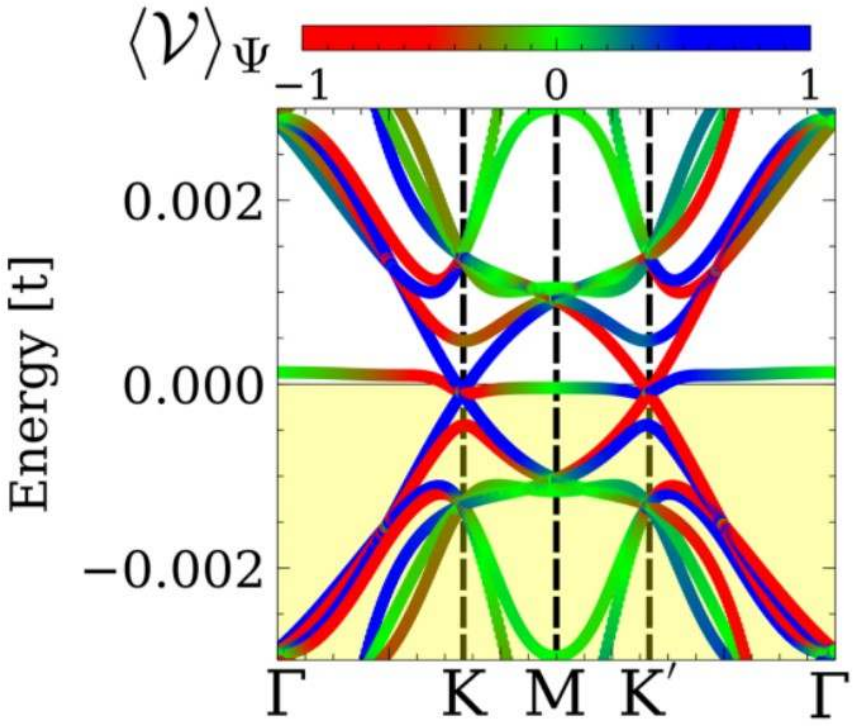

Spatial distribution of the low energy states

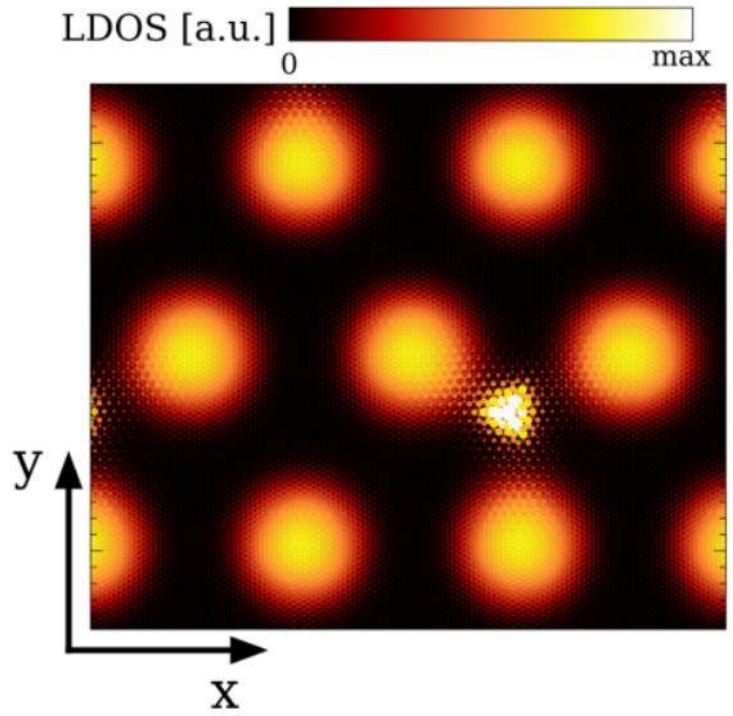

The nearly flat bands coexist with a localized vacancy state

Including interactions in a minimal way

We will include interactions with a minimal Hubbard repulsion

$$H_U = \sum_i U c^\dagger_{i,\uparrow} c_{i,\uparrow} c^\dagger_{i,\downarrow} c_{i,\downarrow} = \sum_i U n_{i,\uparrow} n_{i,\downarrow}$$

Solved at the mean-field level

$$H_U^{\mathrm{MF}} = \sum_i U [\langle n_{i,\uparrow} \rangle n_{i,\downarrow} + \langle n_{i,\downarrow} \rangle n_{i,\uparrow} - \langle n_{i,\uparrow} \rangle \langle n_{i,\downarrow} \rangle]$$

Let us see the impact on the low energy states

Impact of interactions, pristine system

Band structure

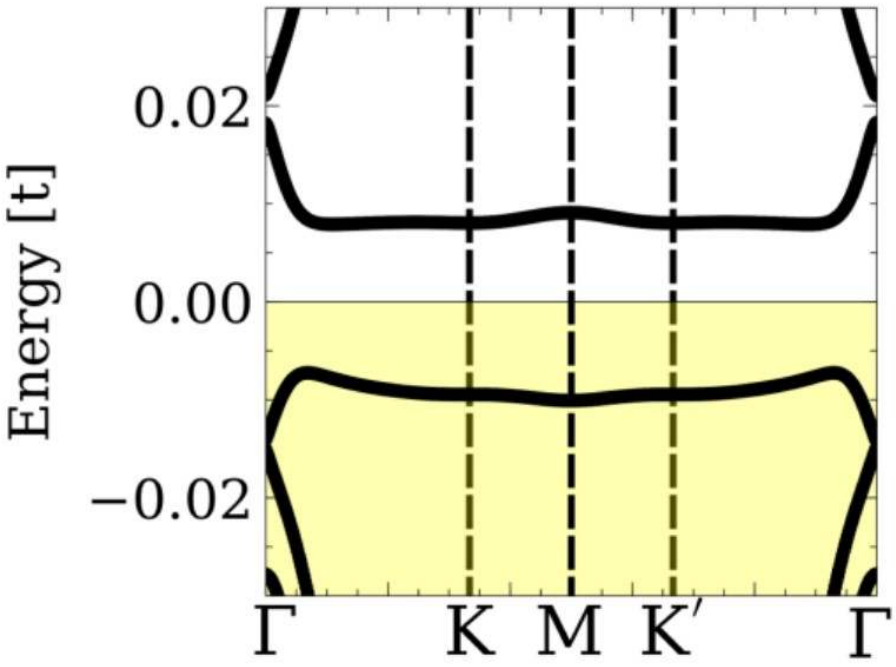

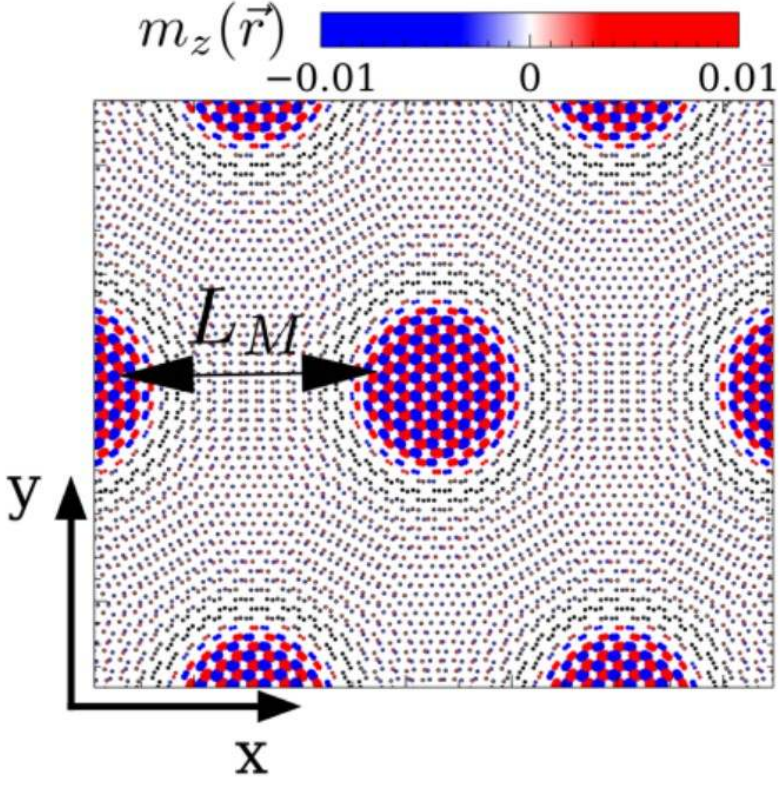

Gap opening at charge neutrality

Impact of interactions, single vacancy at charge neutrality

Band structure

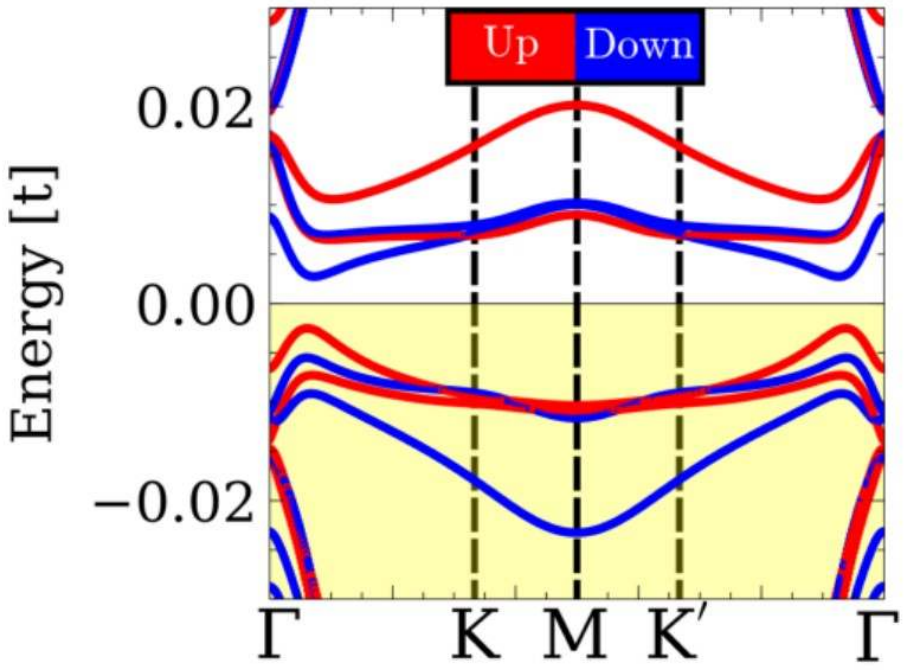

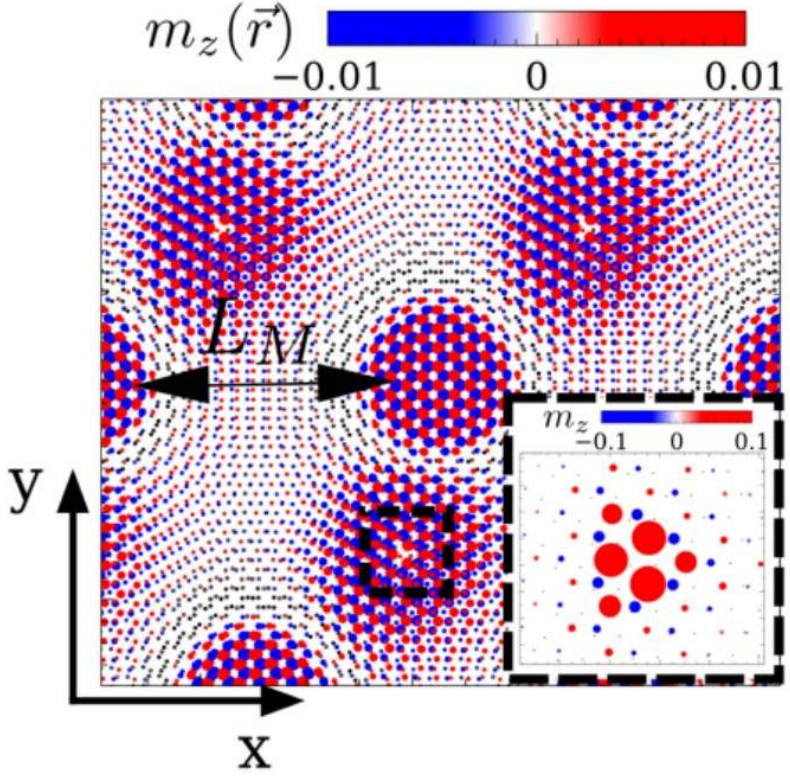

Interaction-driven symmetry breaking in the impurity and flat bands coexists

Impact of interactions, single vacancy at 4e per moire unit cell

Band structure

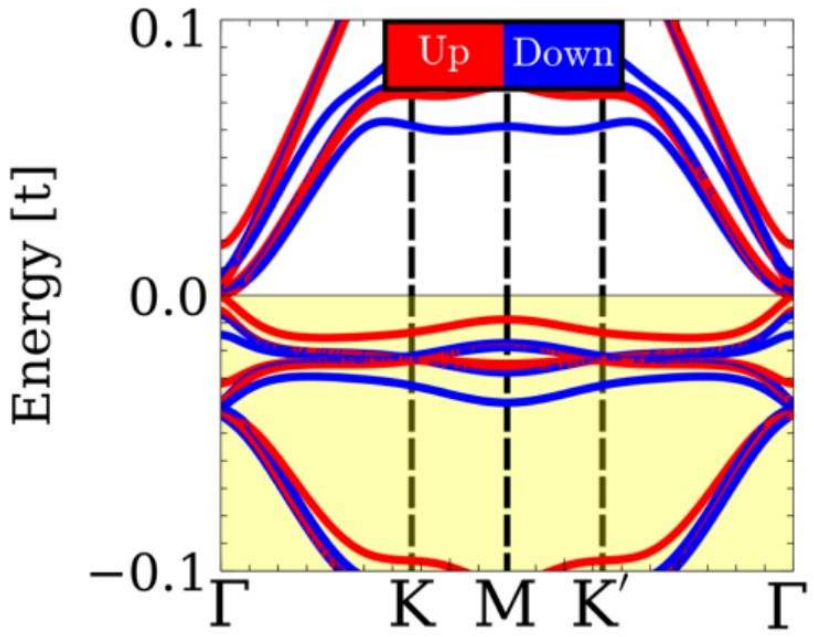

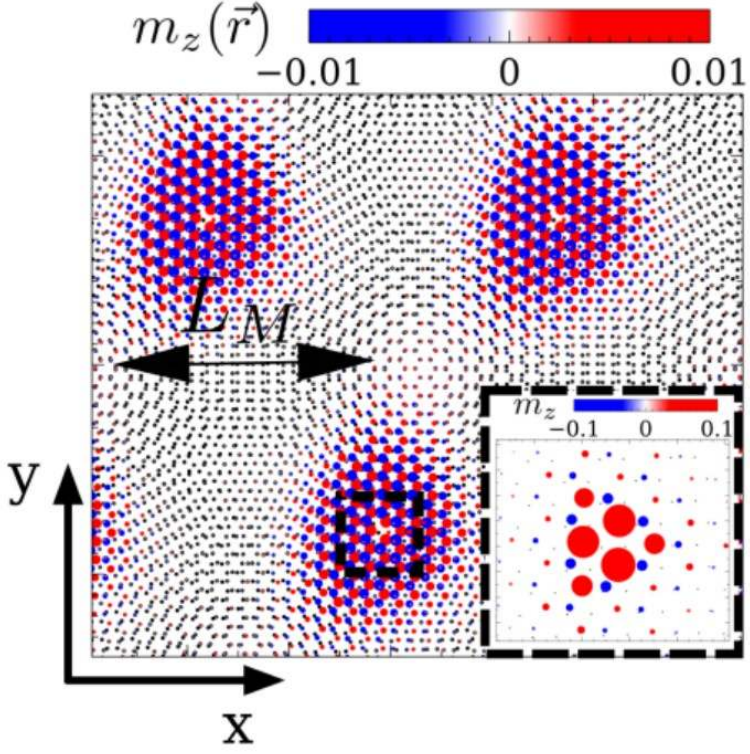

The vacancy magnetism survives full filling of the original twisted bilayer flat bands

Interplay between impurity magnetism and twisted bilayer superconductivity

The impurity induced moment survives doping of the flat bands

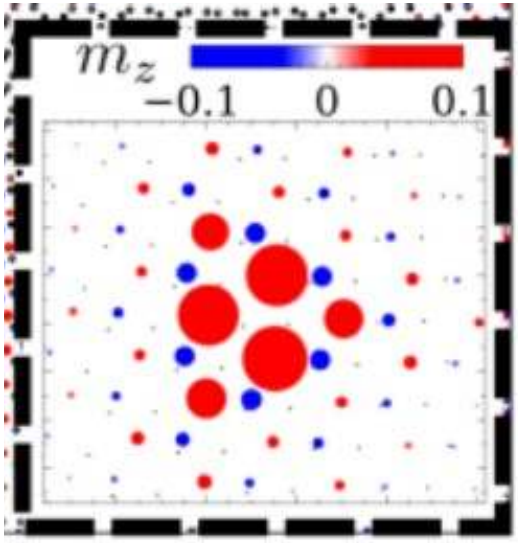

What happens when its magnetism coexists with the twisted bilayer superconducting state?

We will now include a superconducting state

$$H_{\mathrm{SC}} = \sum_i \Delta_i [c_{i,\uparrow} c_{i,\downarrow} + c^\dagger_{i,\downarrow} c^\dagger_{i,\uparrow}]$$

Working in the regime of (close to) 2 holes per moire unit cell

Electronic structure without including interactions

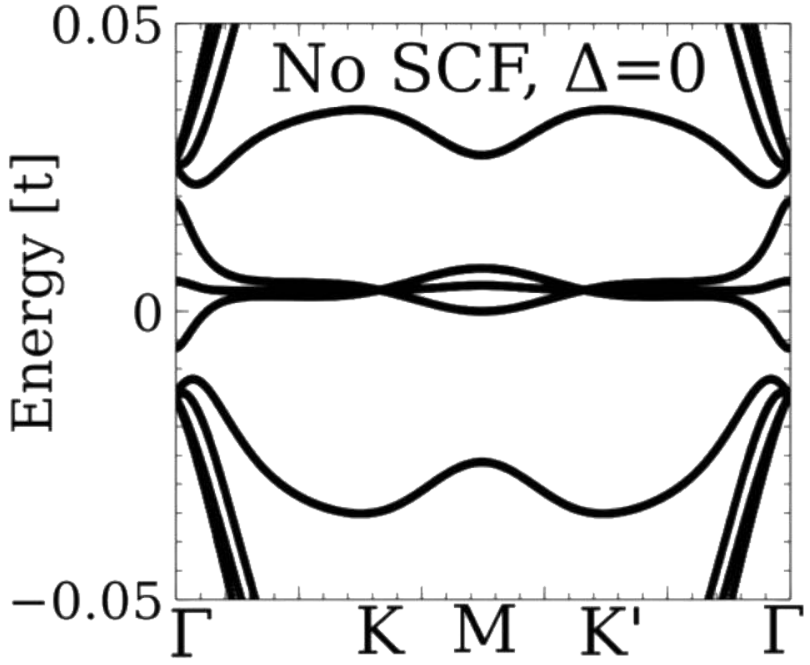

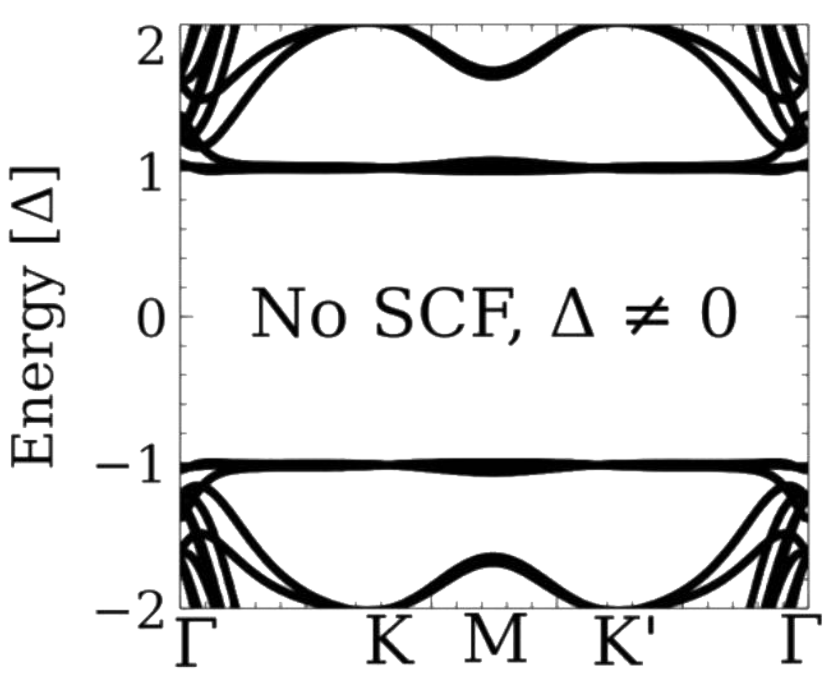

s-wave superconductivity opens up a gap in the electronic spectra

Electronic structure including repulsive interactions

With interaction-induced magnetism

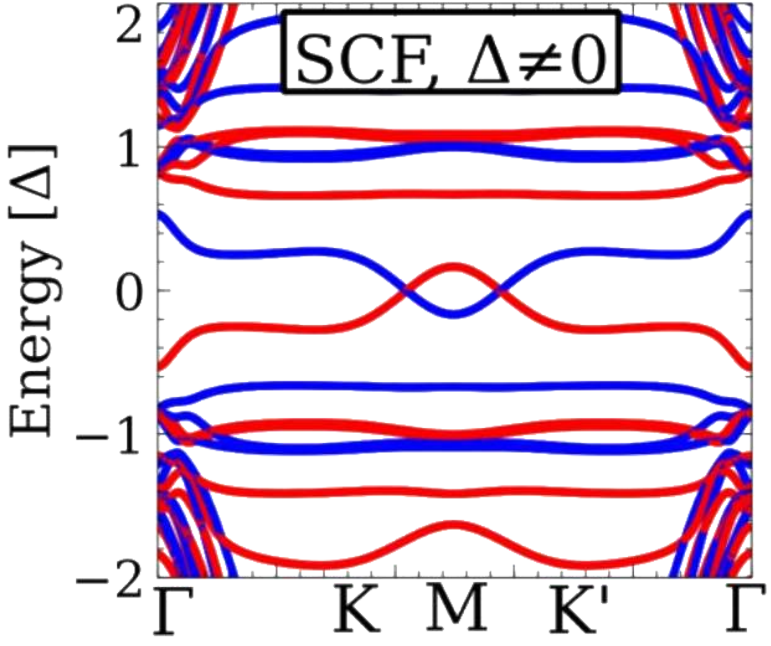

Without interaction-induced magnetism

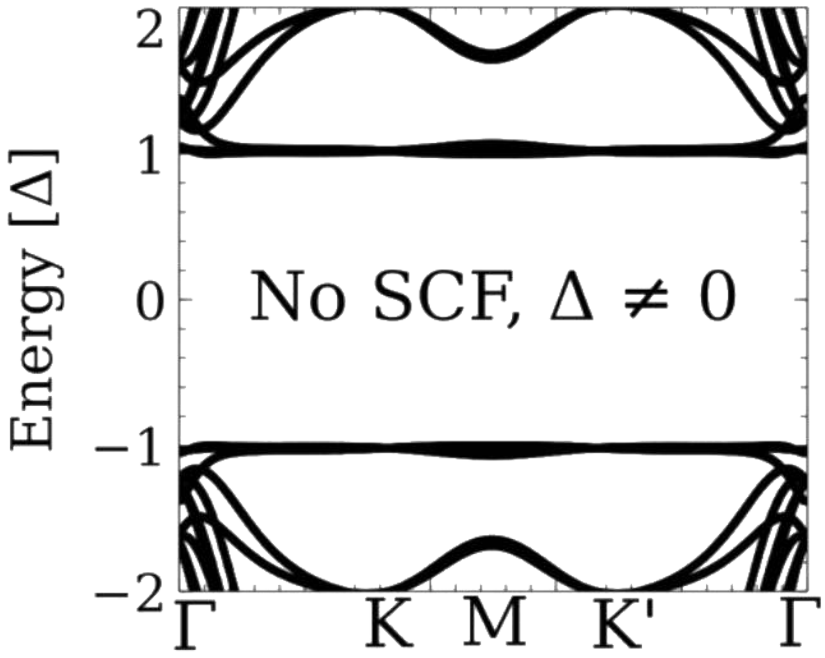

Impurity-induced magnetism and s-wave superconductivity gives rise to in-gap Yu-Shiba-Rusinov states

Electronic structure including repulsive interactions

With interaction-induced magnetism

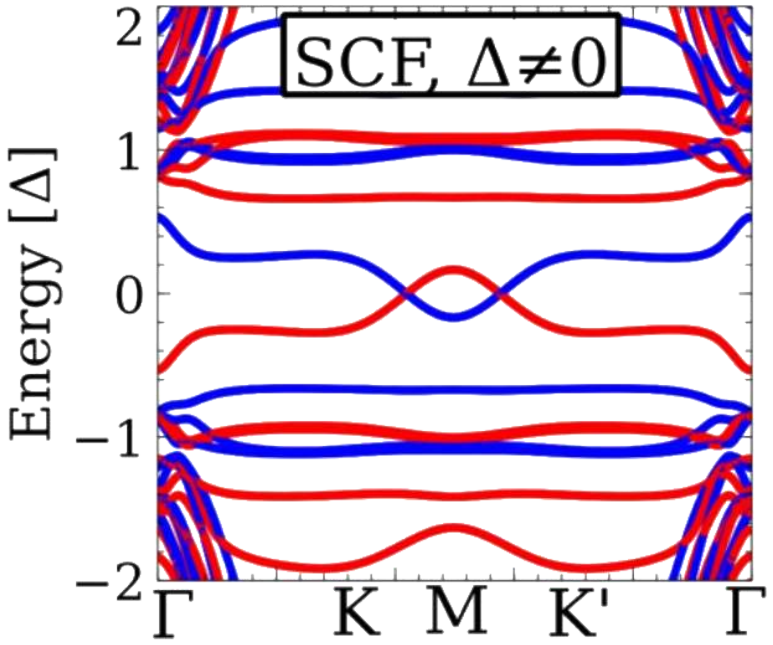

Spatial distribution of the in-gap YSR states

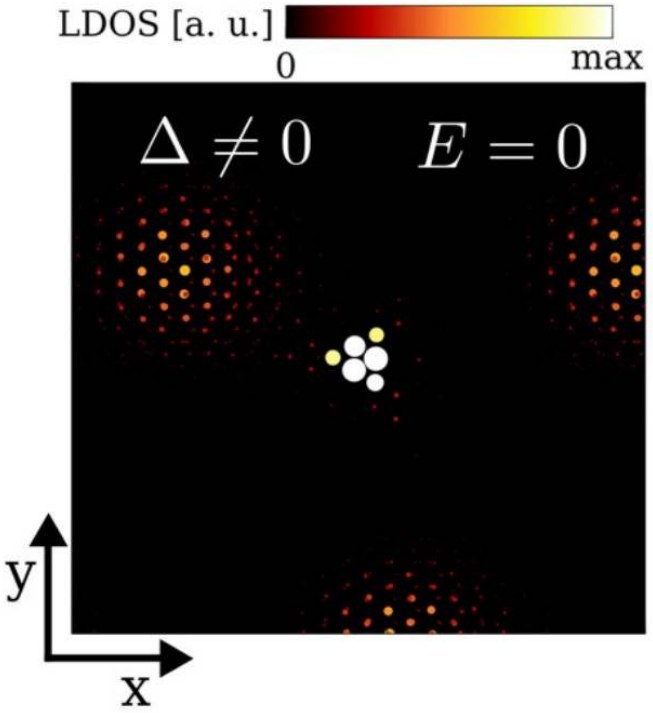

In-gap modes appear around the interaction-induced impurity magnetic moment

Impurities in twisted trilayer graphene

Structure of mirror-symmetric twisted graphene trilayer

Top view

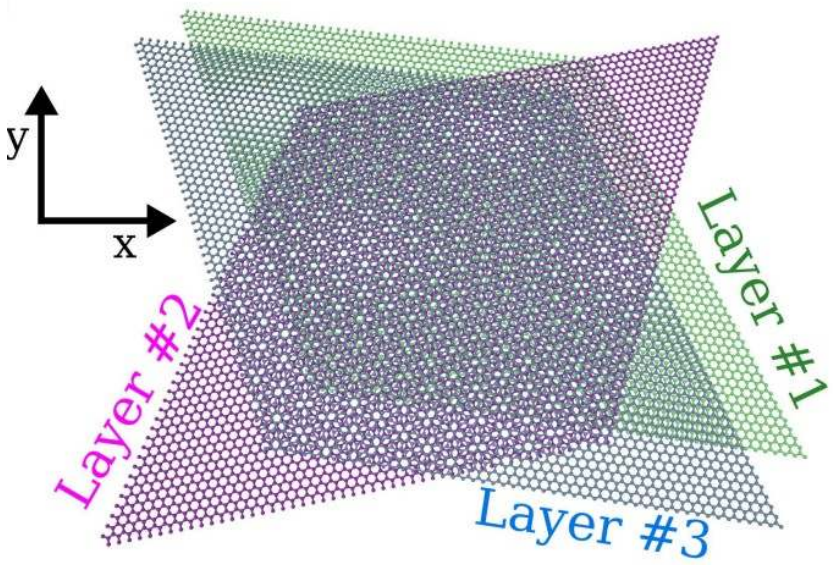

Lateral view

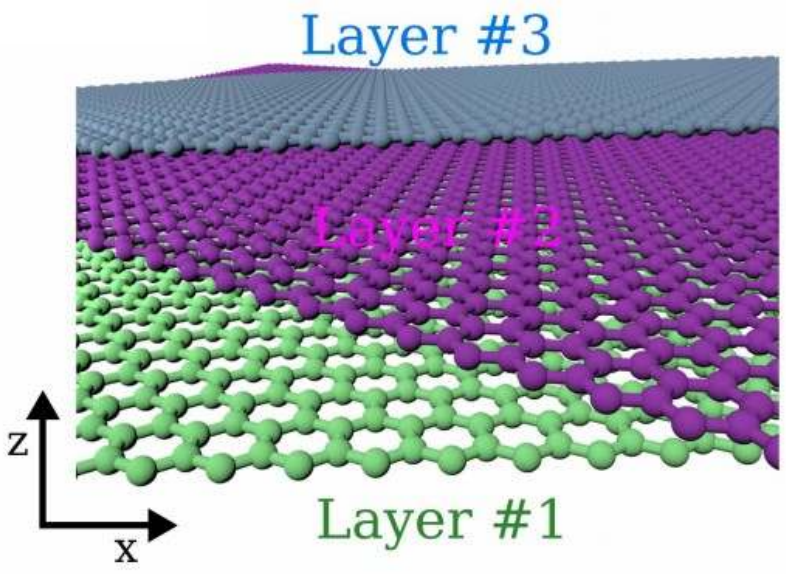

DFT electronic structure of twisted trilayer graphene

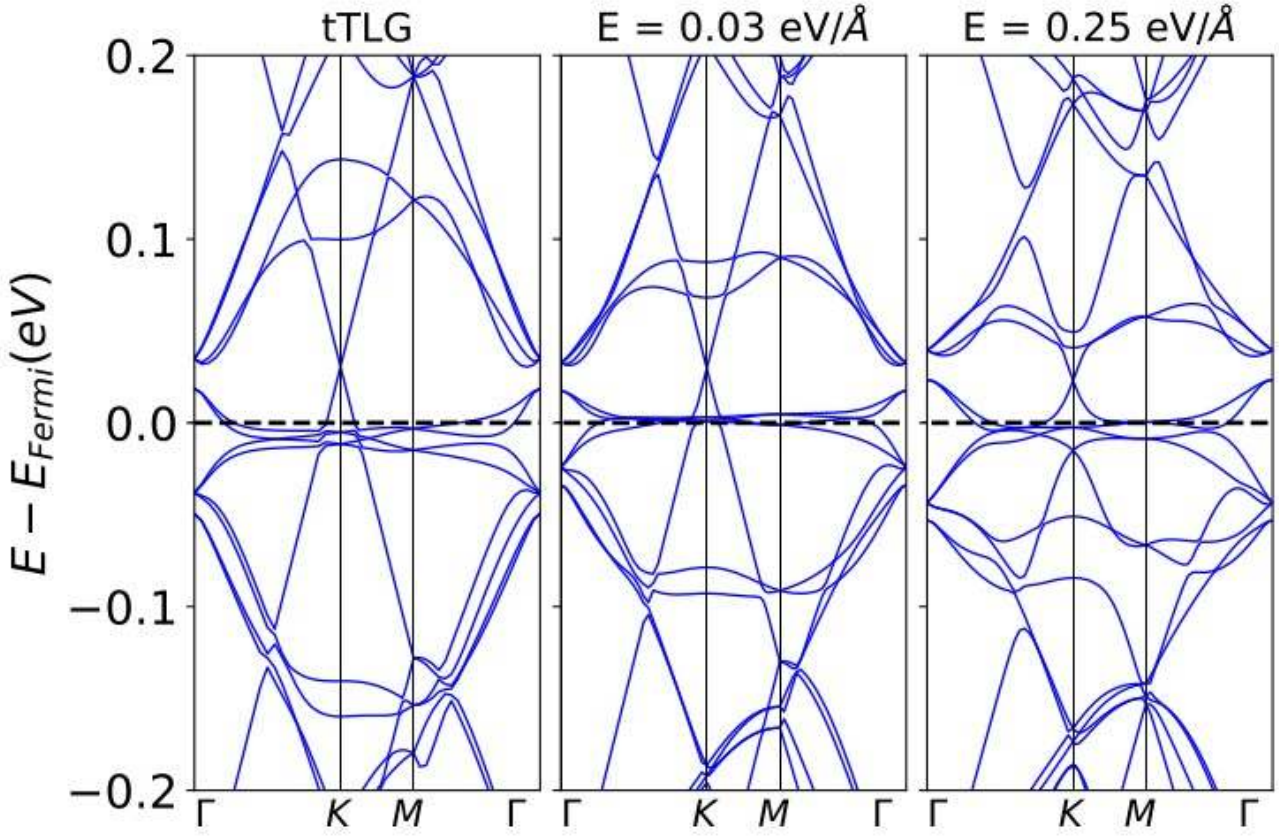

1.9 degrees

DFT electronic structure of twisted trilayer graphene

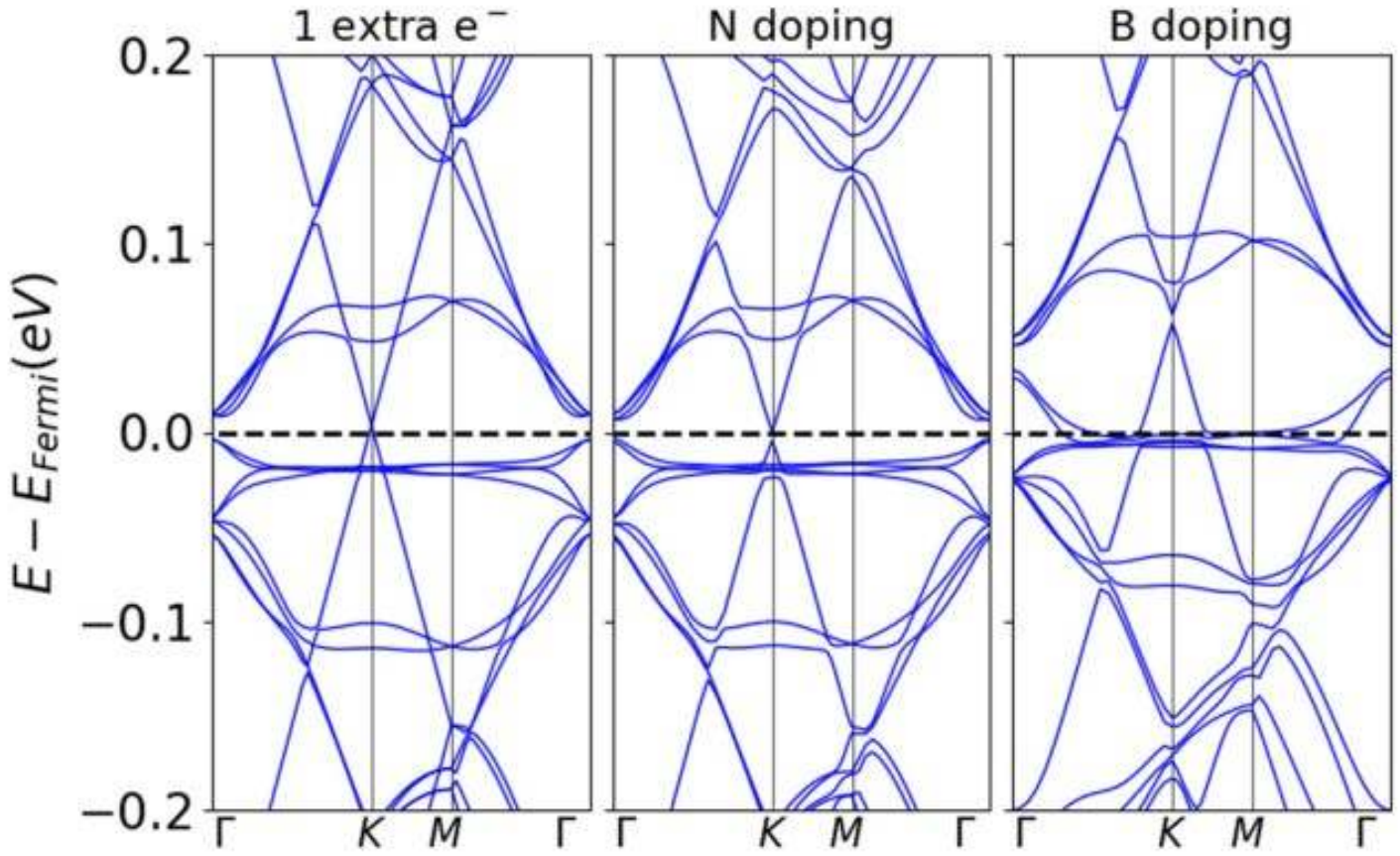

1.9 degrees

A technical note: impurities and valley mixing

Do B/N/H impurities influence the valley degree of freedom?

The valley operator

$$\mathcal{V}_z = \frac{i}{3\sqrt{3}} \sum_{\langle\langle i,j \rangle\rangle, s} \eta_{ij} \sigma_z^{ij} c_{i,s}^{\dagger} c_{j,s},$$

Allows to compute valley in a real-space graphene model

The local valley current operator

$$\chi_V(\mathbf{r}, \omega) = \int \frac{d^2\mathbf{k}}{(2\pi)^2} \frac{\epsilon_{\alpha\beta}}{2} \langle \mathbf{r} | G_V \left(\partial_{k_\alpha} G_V^{-1}\right) \left(\partial_{k_\beta} G_V\right) | \mathbf{r} \rangle \qquad G_V = [\omega - \mathcal{H}_{\mathbf{k}} + i0^+]^{-1} \mathcal{V}_z$$

Allows to image valley currents (and mixing) in a real space tight binding model

The valley operator for monolayer graphene

1x1 unit cell

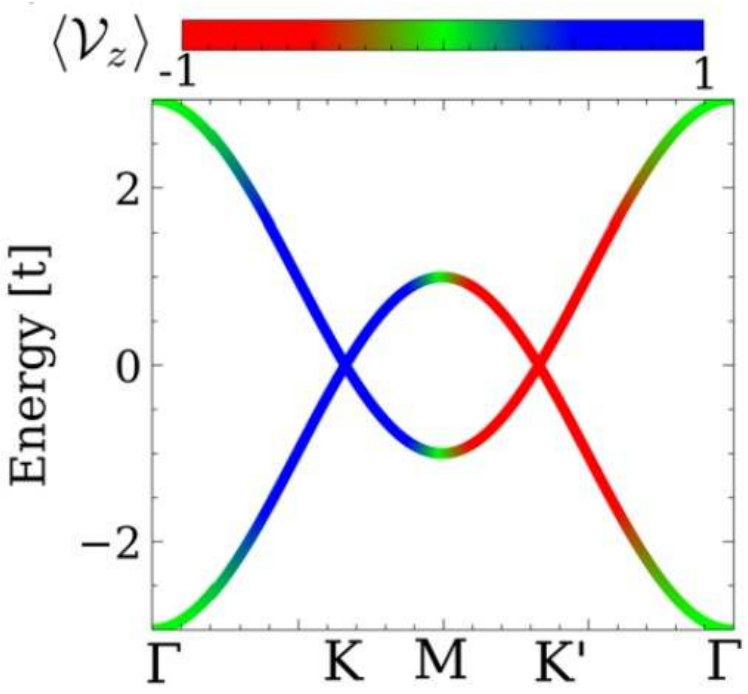

8x8 unit cell

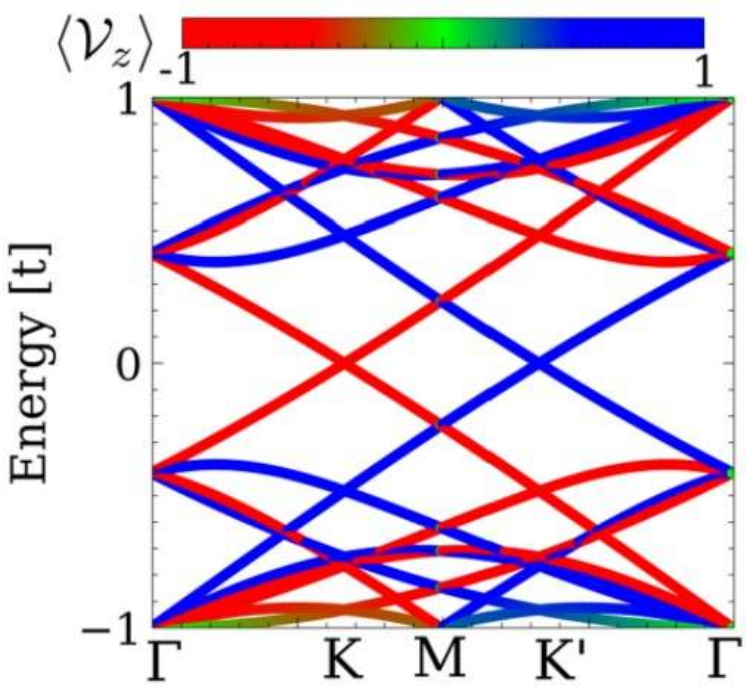

The valley operator

Graphene zigzag nanoribbon

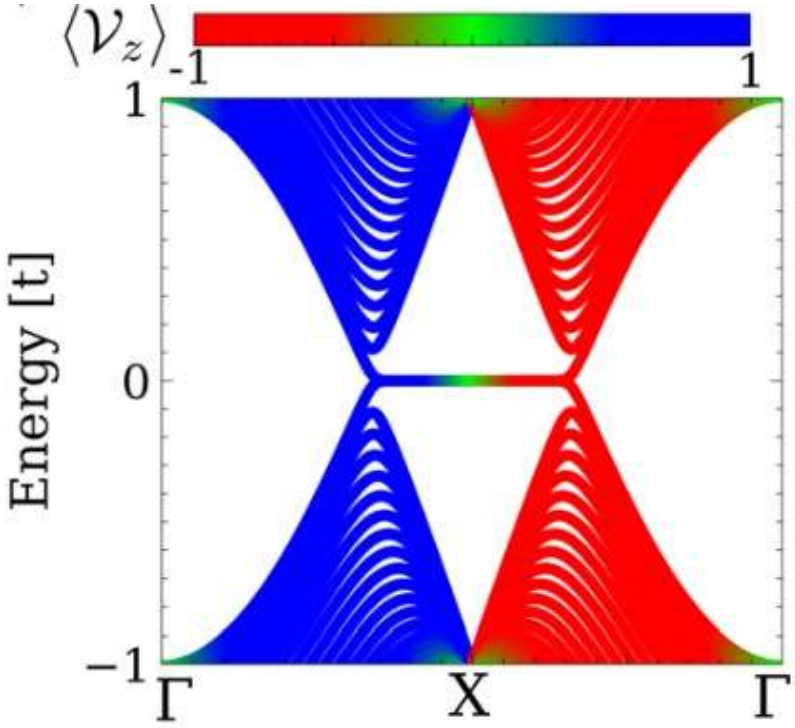

Biased AB bilayer graphene

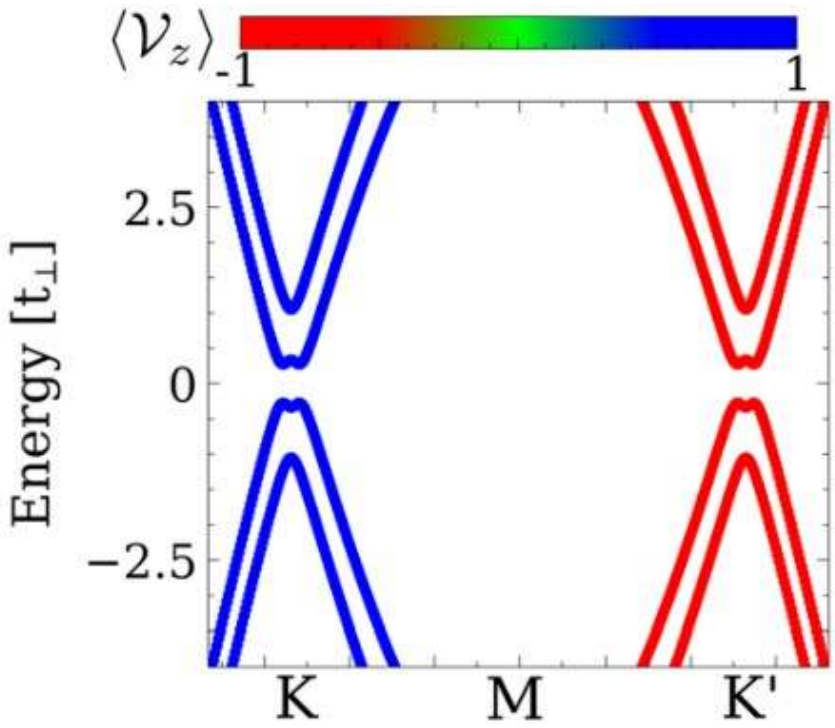

Electronic structure of twisted trilayer

Without an interlayer bias

With an interlayer bias

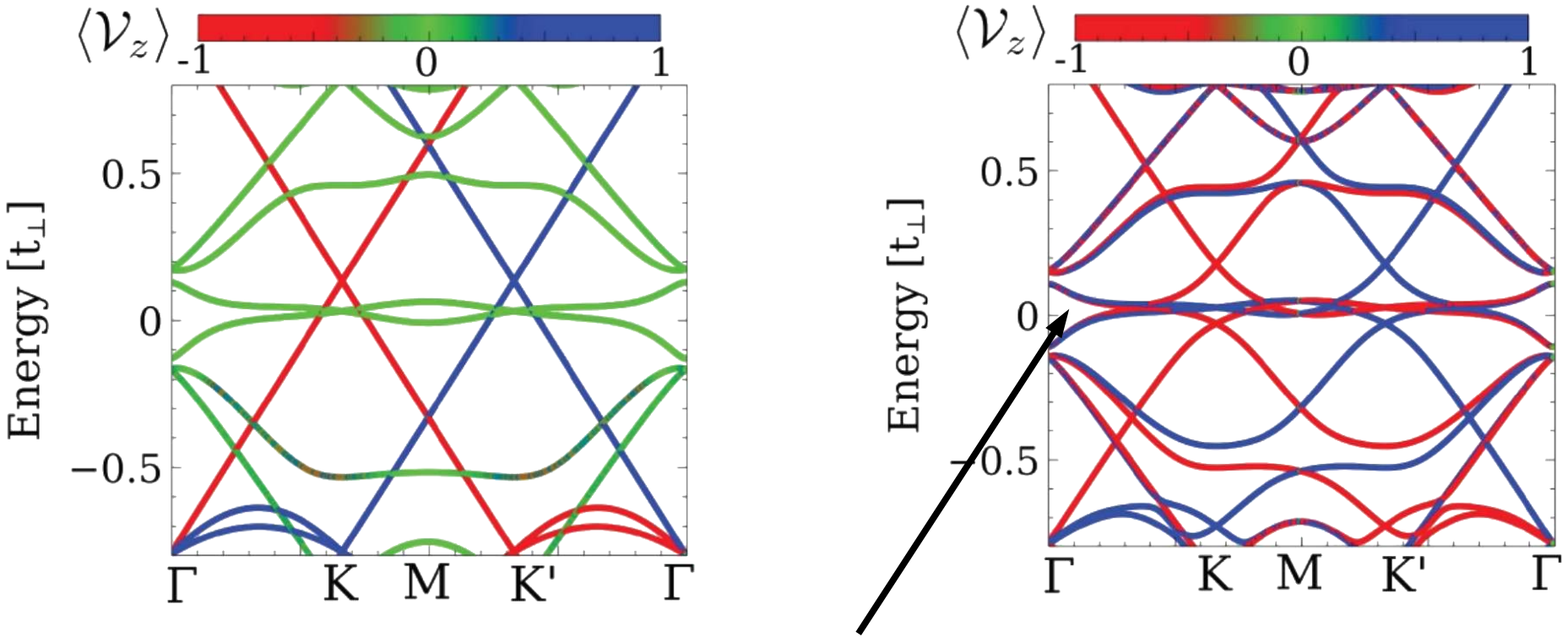

An interlayer bias creates internal topological valley currents

Internal topological valley currents in a twisted trilayer

The spatially resolved valley current is defined from the valley Chern number

$$C_V = C_K - C_{K'} = \int \chi_V(\mathbf{r}, \omega) d^2\mathbf{r}\, d\omega$$

Spatially and frequency resolved valley Chern density

$$\chi_V(\mathbf{r}, \omega)$$

It represents bulk valley currents

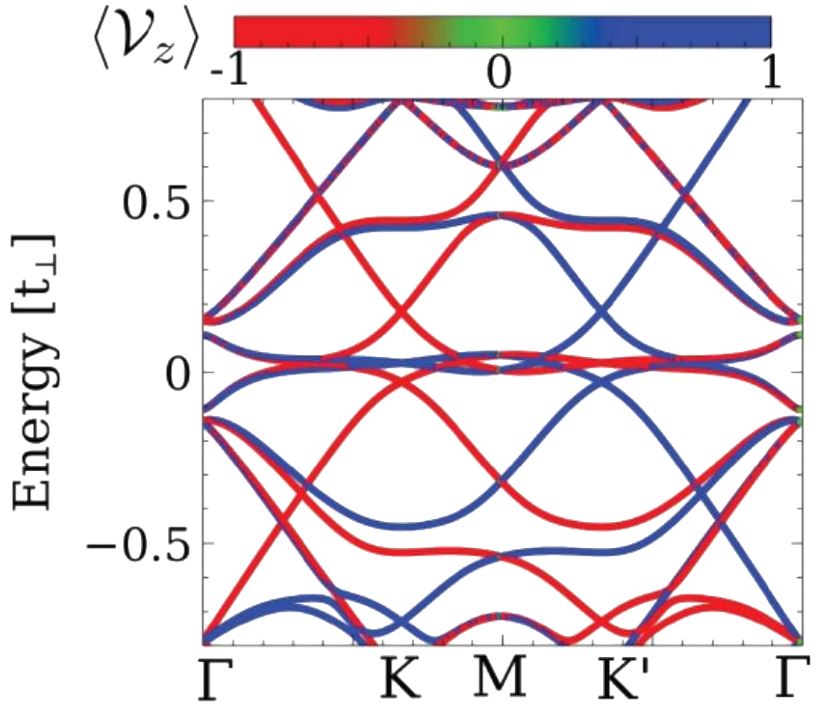

Internal topological valley currents in a twisted trilayer

Bulk valley current

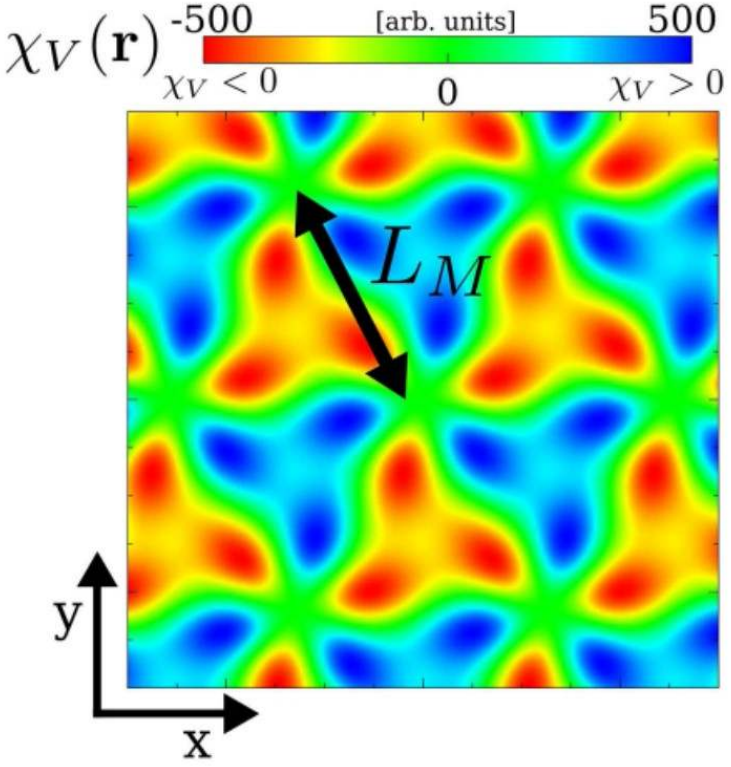

Band structure

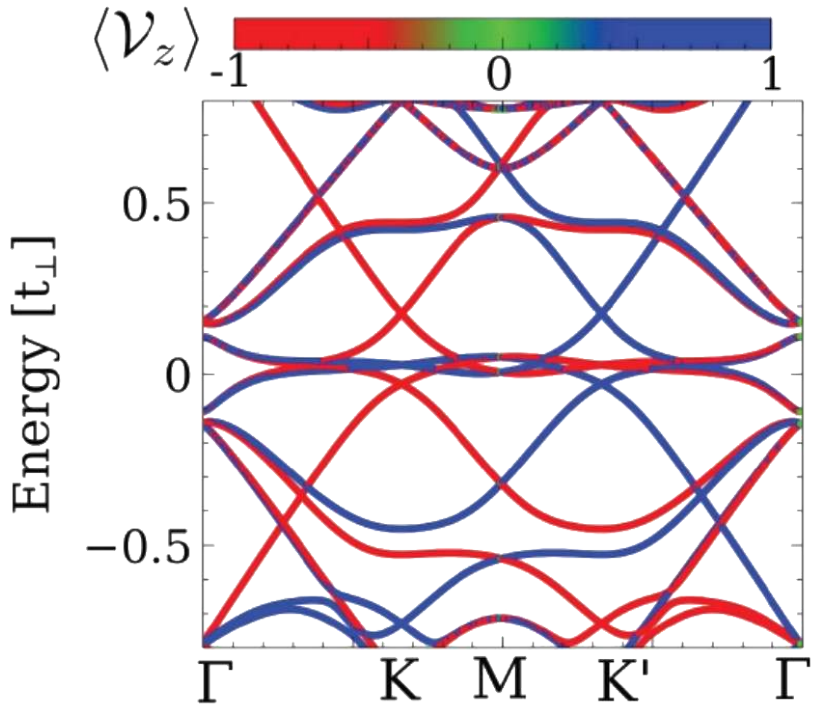

Internal topological valley currents emerge in the moire supercell

Weak impurity in a twisted graphene trilayer

Bulk valley current

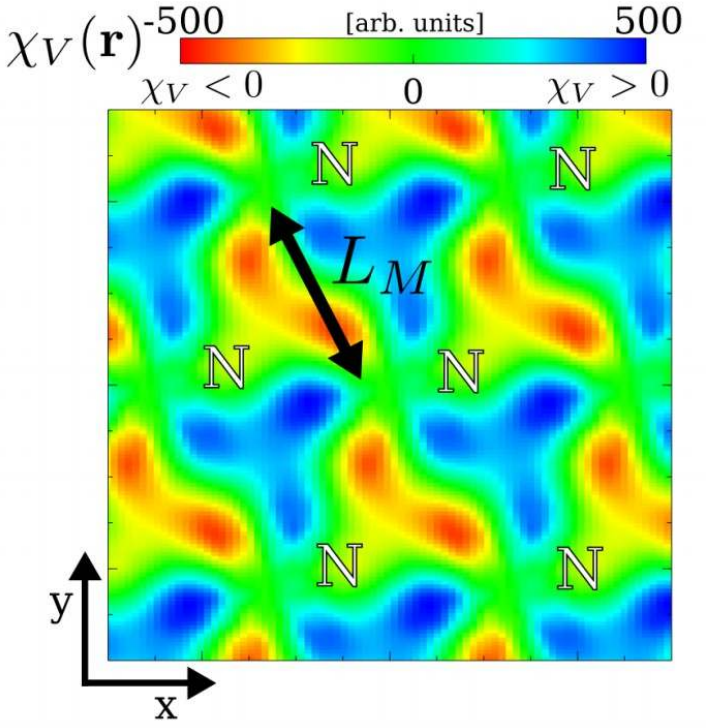

Band structure

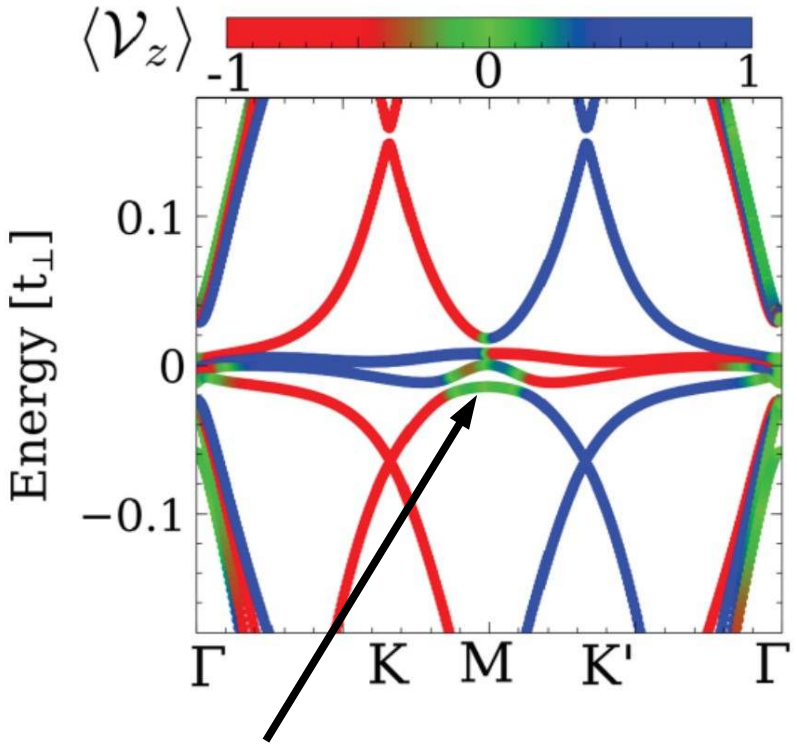

Weak impurities give rise to valley mixing at low energies

Disruption of valley currents by an impurity

Pristine

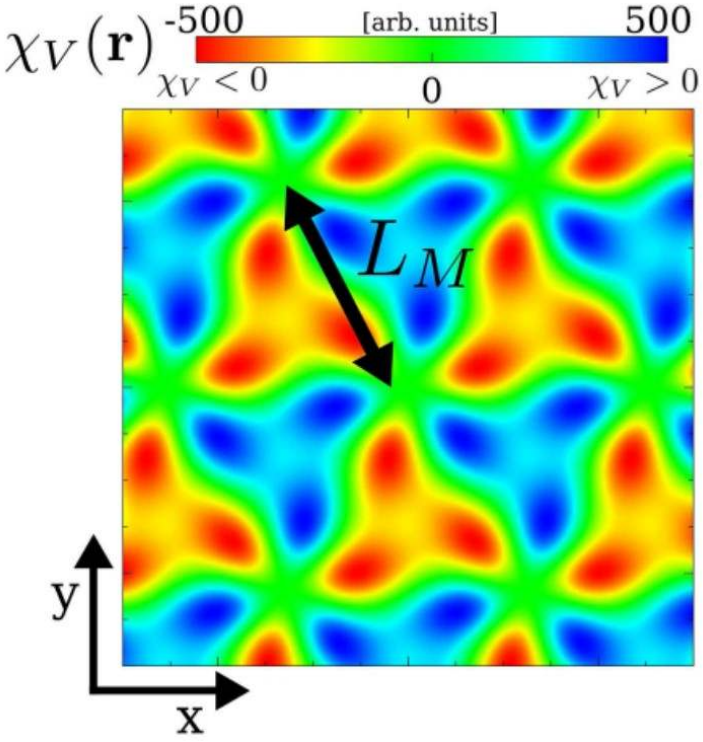

Weak impurity

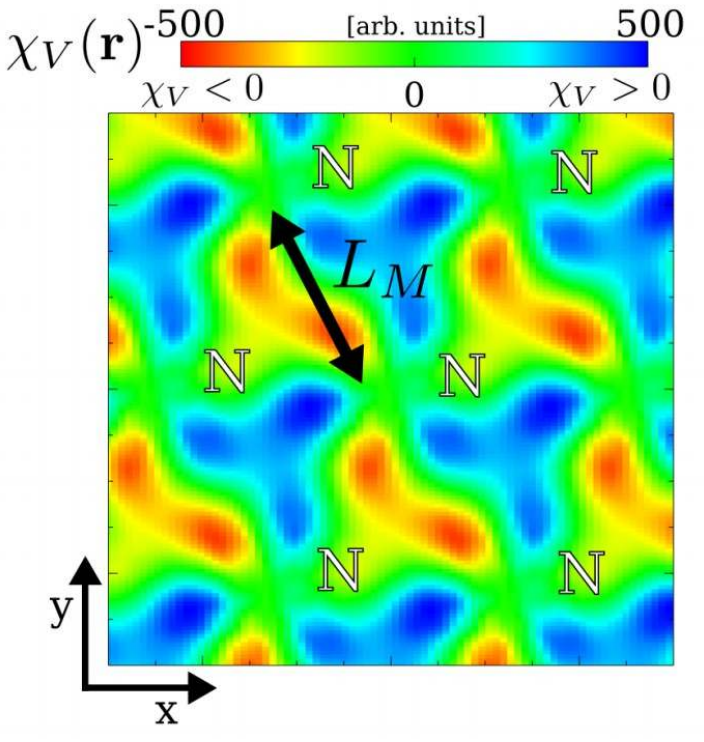

Weak impurities disrupt the valley currents in twisted graphene trilayers

Impurities in a twisted topological superconductor

Topological superconductors

Full gap in the bulk

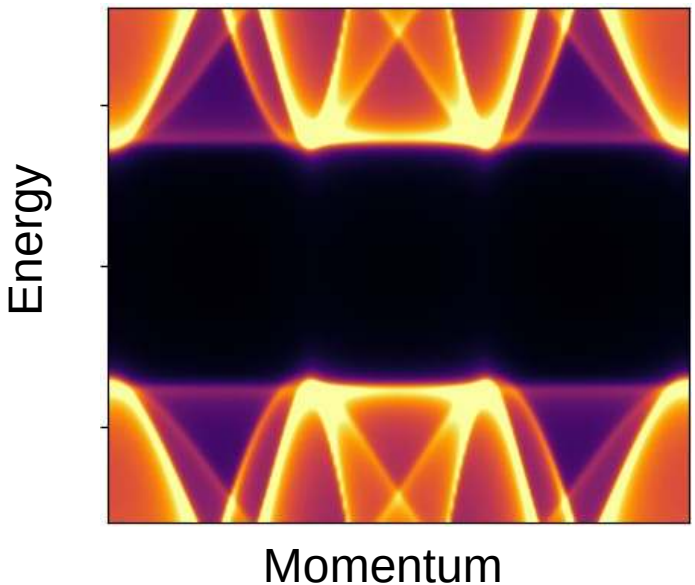

Gapless (Majorana) mode
at the edge

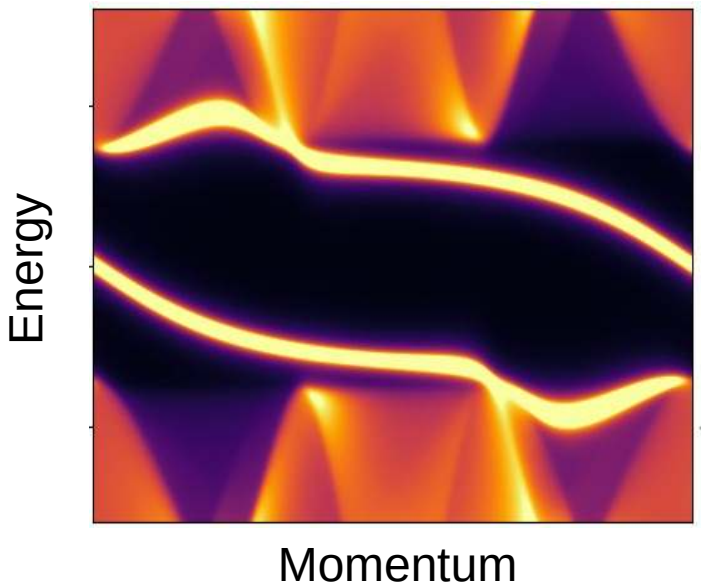

Topological superconductors are rare in nature, and thus have to be artificially engineered

Topological superconductivity in a van der Waals heterostructure

$CrBr_3/NbSe_2$ heterostructure

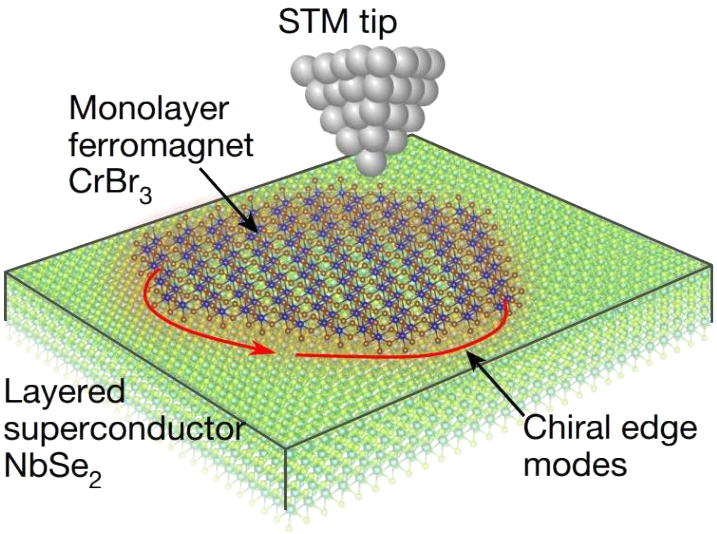

Zero bias dI/dV

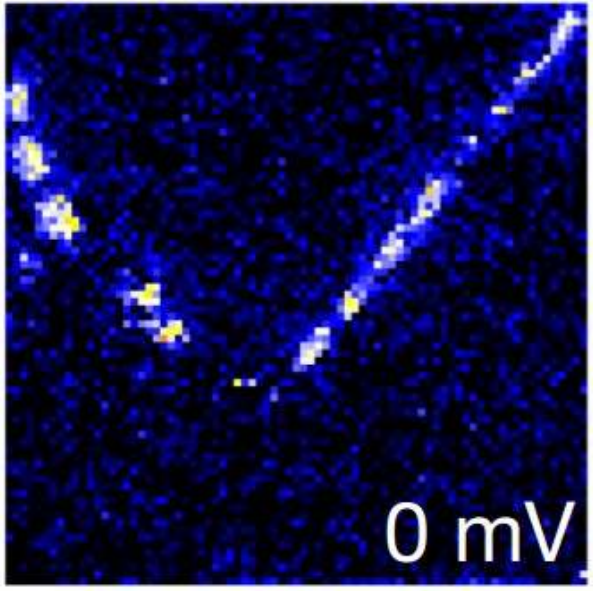

Nature 588, 424–428 (2020)

A topological superconducting state appears in $CrBr_3/NbSe_2$

Topological superconductivity in $CrBr_3/NbSe_2$ heterostructure

$CrBr_3/NbSe_2$ heterostructure

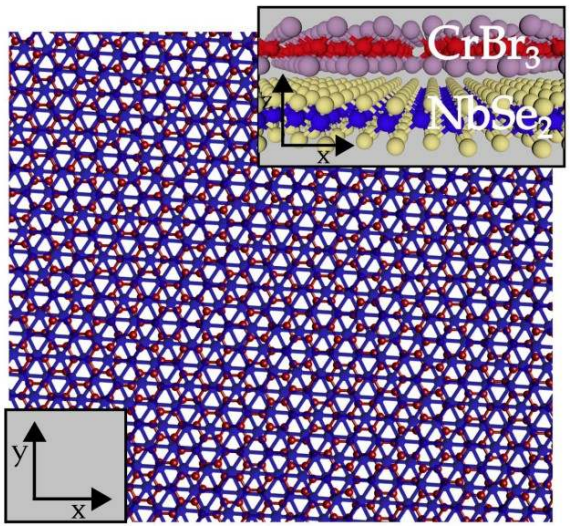

Nature 588, 424–428 (2020)
Nano Lett. 2022, 22, 1, 328–333

Zero bias dIdV

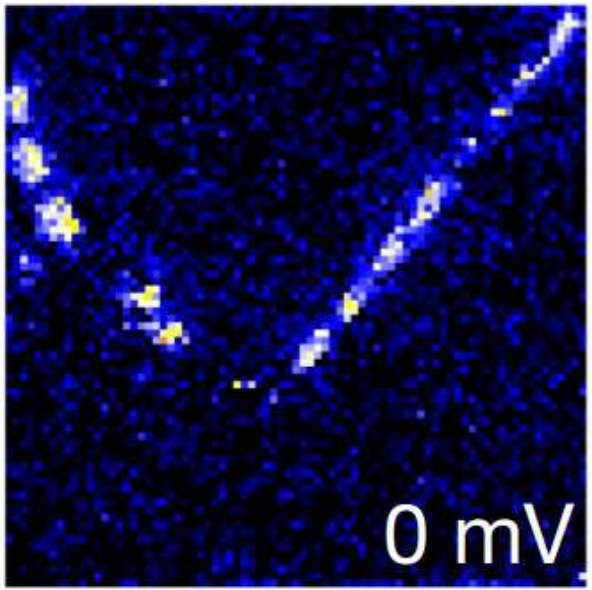

A topological superconducting state appears in $CrBr_3/NbSe_2$

$CrBr_3/NbSe_2$ heterostructure

Topography

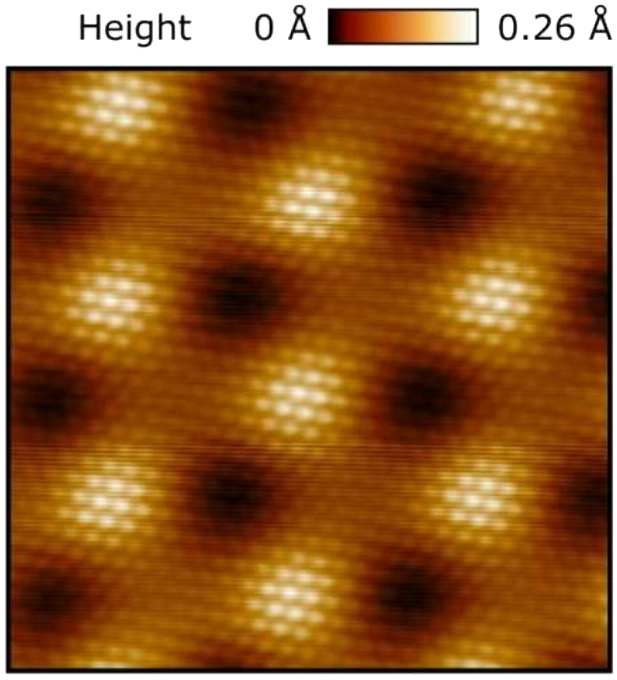

dIdV of the Yu-Shiba-Rusinov states

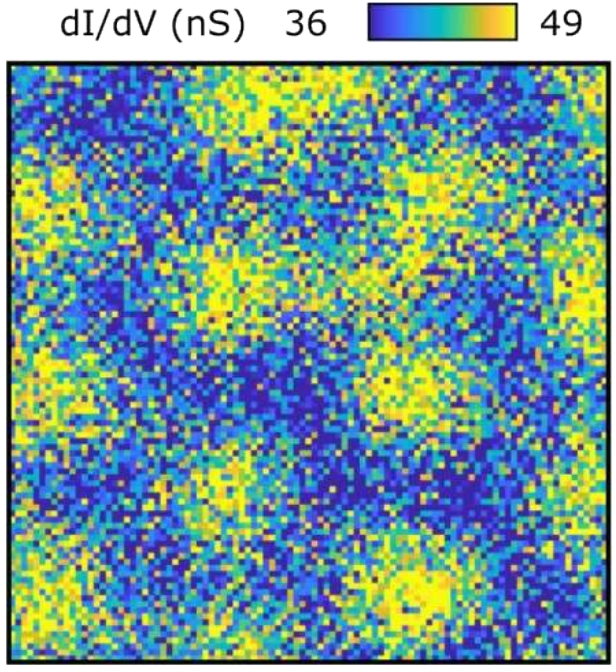

The low energy properties are affected by the moire pattern

Hamiltonian for the pristine moire topological superconductor

Structure

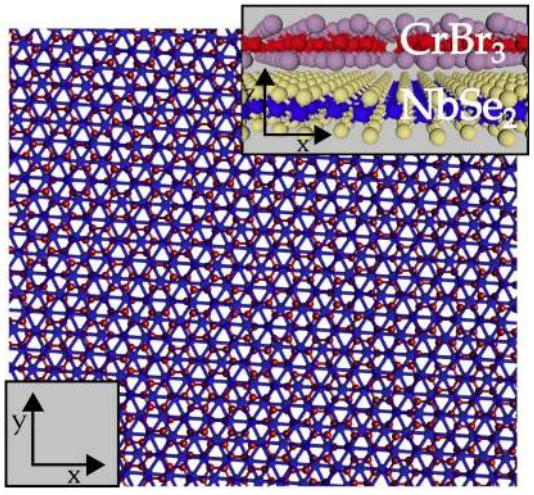

Exchange profile

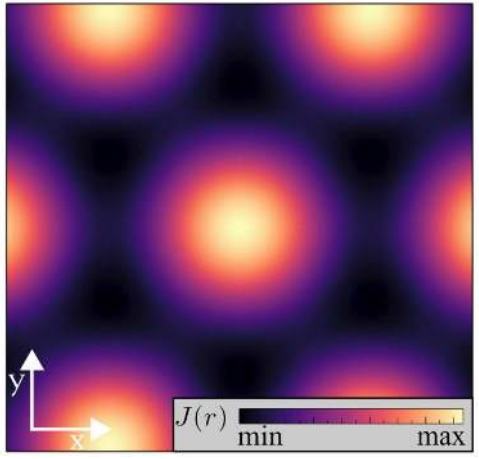

Superconducting profile

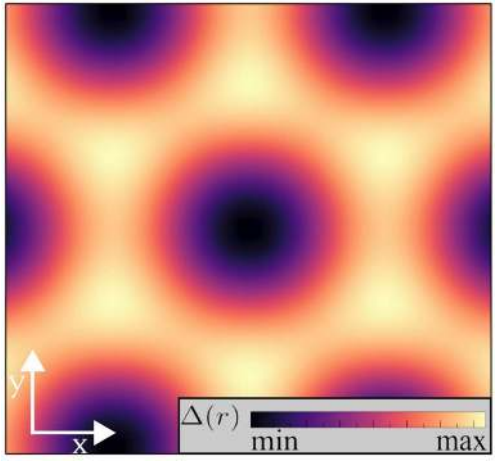

$$\mathcal{H}_0 = \mathcal{H}_{\text{kin}} + \mathcal{H}_J + \mathcal{H}_R + \mathcal{H}_{\text{SC}}$$

Kinetic energy

Exchange coupling

Rashba SOC

s-wave superconductivity

Hamiltonian for the defective moire topological superconductor

Full Hamiltonian

$$\mathcal{H} = \mathcal{H}_0 + \mathcal{H}_{\text{imp}}$$

Local impurity in the moire system

$$\mathcal{H}_{\text{imp}} = w \sum_s c^\dagger_{n,s} c_{n,s}$$

Weak impurity

$$w \to 0$$

Strong impurity

$$w \to \infty$$

$$\mathcal{H}_0 = \mathcal{H}_{\text{kin}} + \mathcal{H}_J + \mathcal{H}_R + \mathcal{H}_{\text{SC}}$$

Kinetic energy

Exchange coupling

Rashba SOC

s-wave superconductivity

Impurities in the moire topological superconductor

Band structure in the absence of impurity

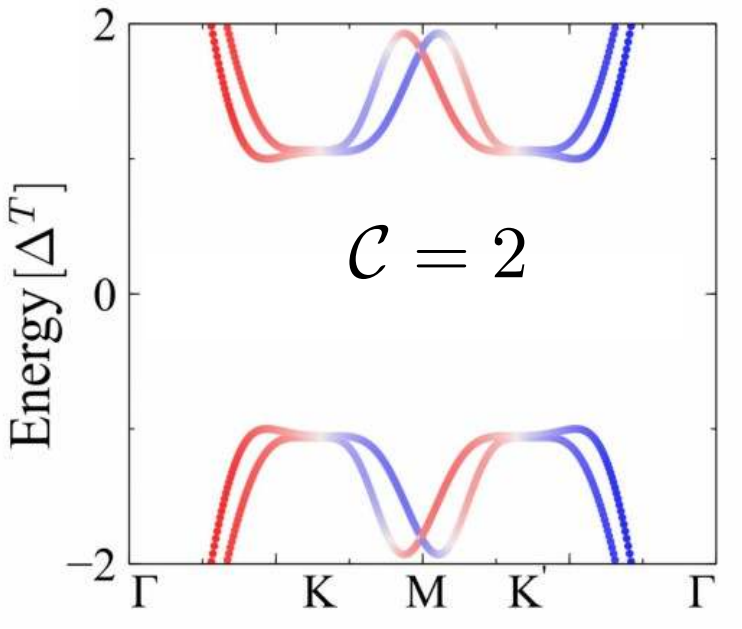

Band structure in the presence of an impurity

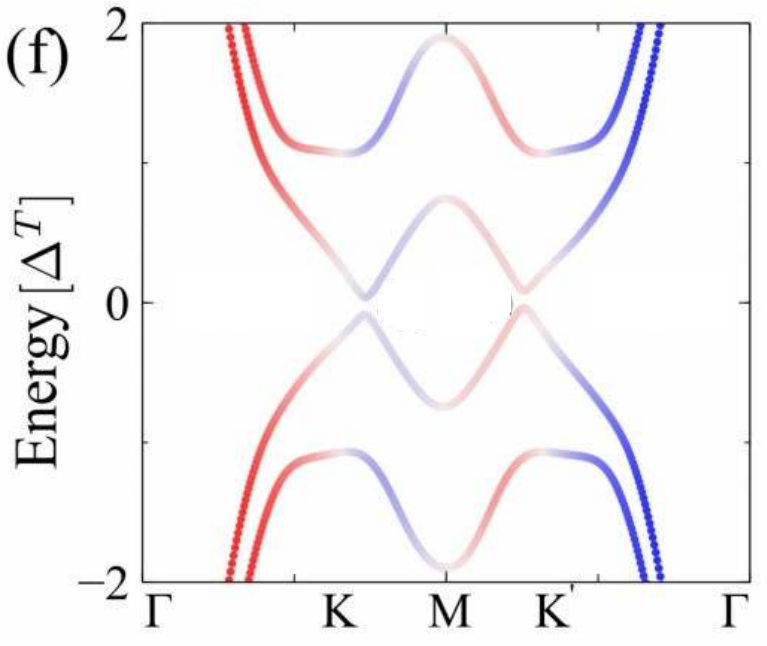

Strong local impurities decrease the size of a topological gap

Gap as a function of the location of a strong impurity

Gap as function of the location of the impurity

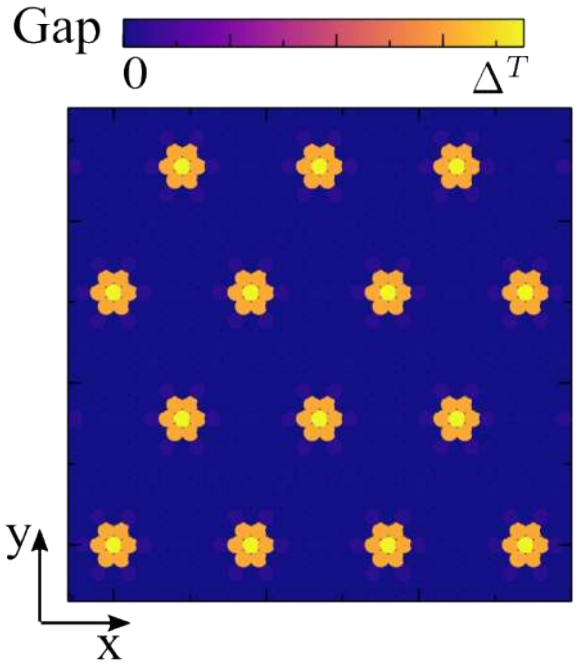

Band structure for impurity at the center

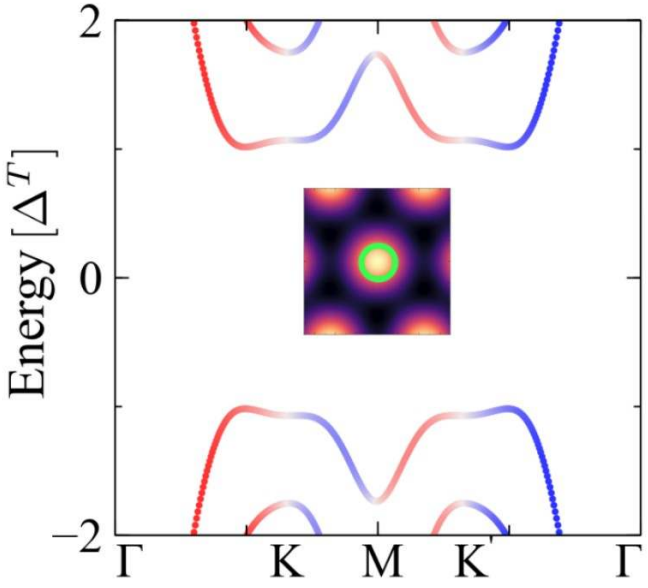

Band structure for impurity away from the center

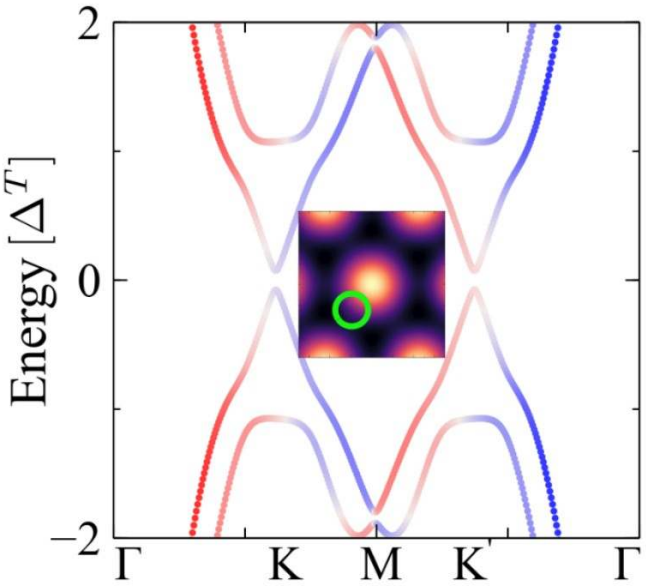

The location of the impurity strongly affects the resulting gap

Gap as a function of the location of a strong impurity

Gap as function of the location of the impurity

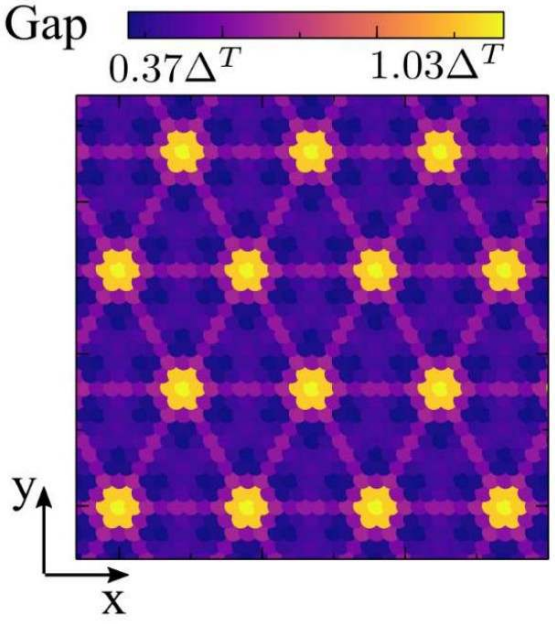

Band structure for impurity at the center

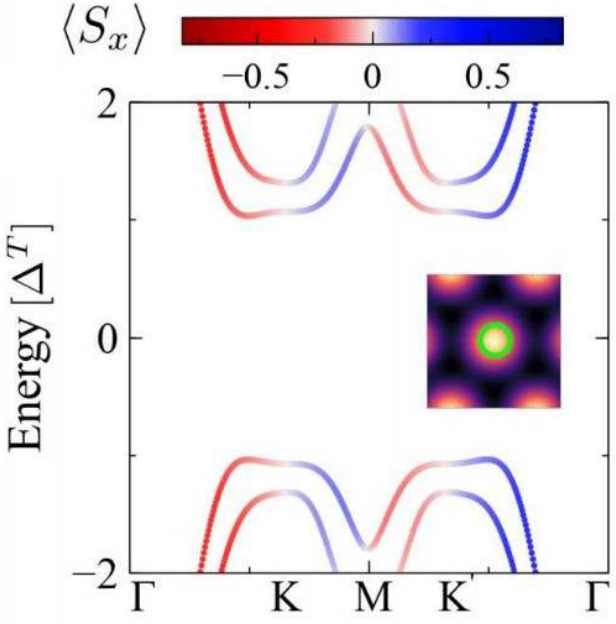

Band structure for impurity away from the center

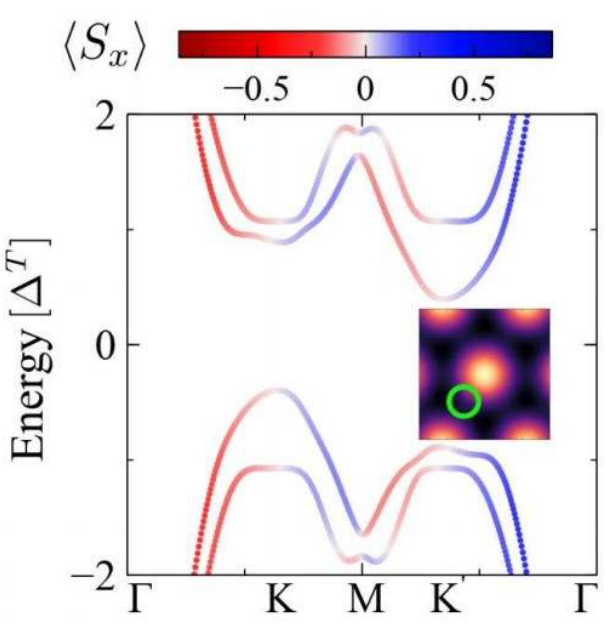

The location of the impurity strongly affects the resulting gap

Gap as function of location for different moire unit cells

11x11 supercell

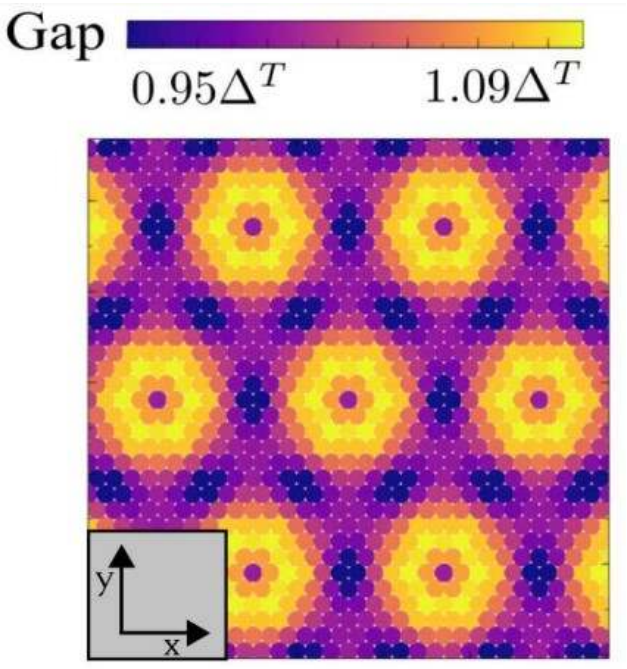

15x15 supercell

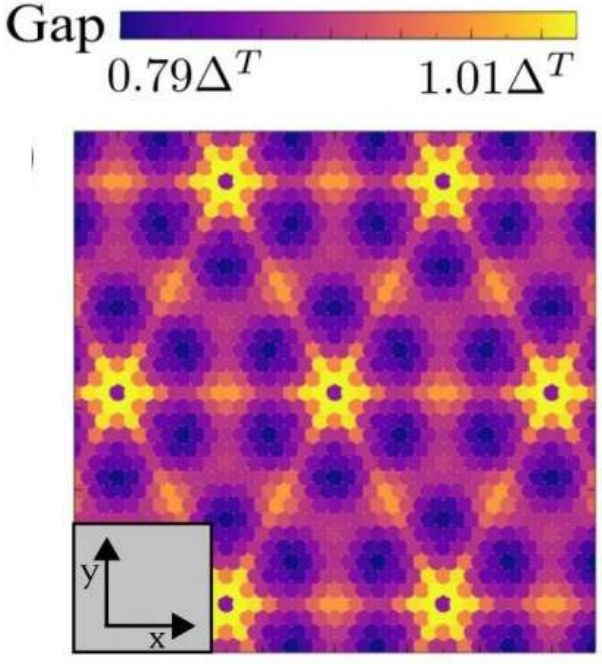

17x17 supercell

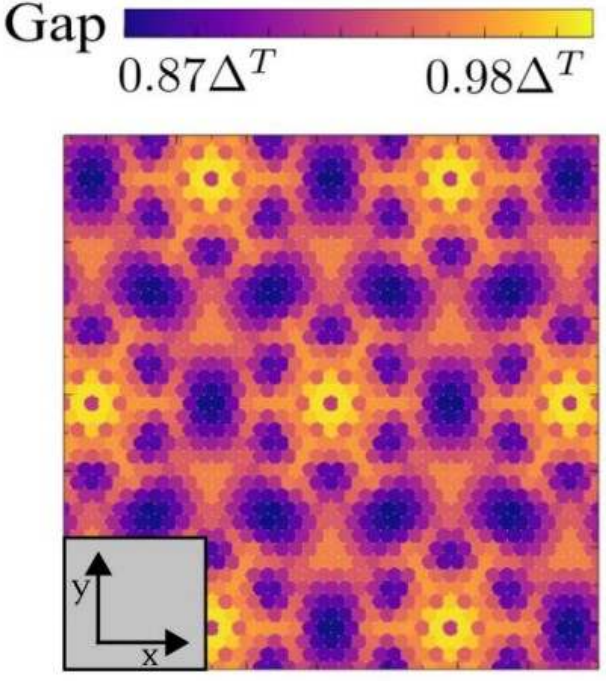

Detrimental locations for impurities depend on the specific moire supercell

The single impurity limit

We now look at the single impurity regime

From the Green's function, we can compute the spatially resolved density of states at the energy of the YSR state

$$\rho(\mathbf{x},\omega) = -\frac{1}{\pi}\sum_{s,\tau}\langle \mathbf{x},s,\tau|\mathrm{Im}(G_V(\omega))|\mathbf{x},s,\tau\rangle$$

Dyson equation for a single impurity

$$G_V(\omega) = [\omega - H_V - \Sigma(\omega) + i0^+]^{-1}$$

Selfenergy from the pristine regime

$$G_0(\omega) = [\omega - H_0 - \Sigma(\omega) + i0^+]^{-1}$$

YSR without moire

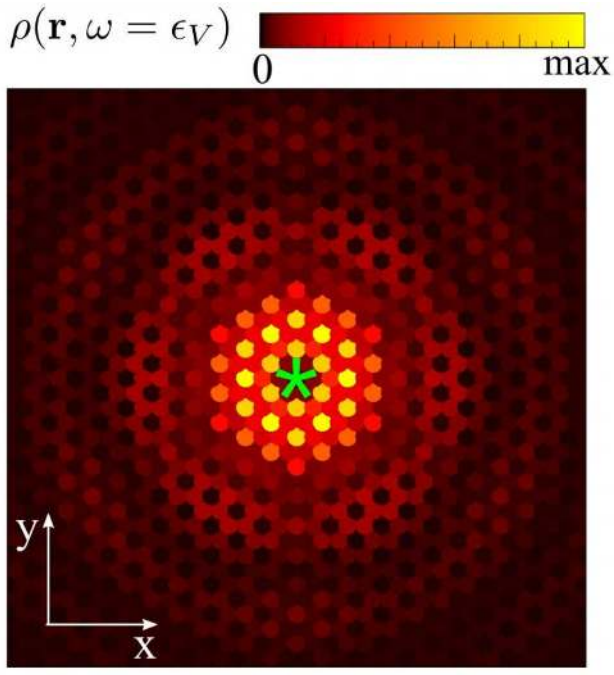

Single impurity in a topological moire superconductor

Wavefunction of the YSR state for different impurity locations

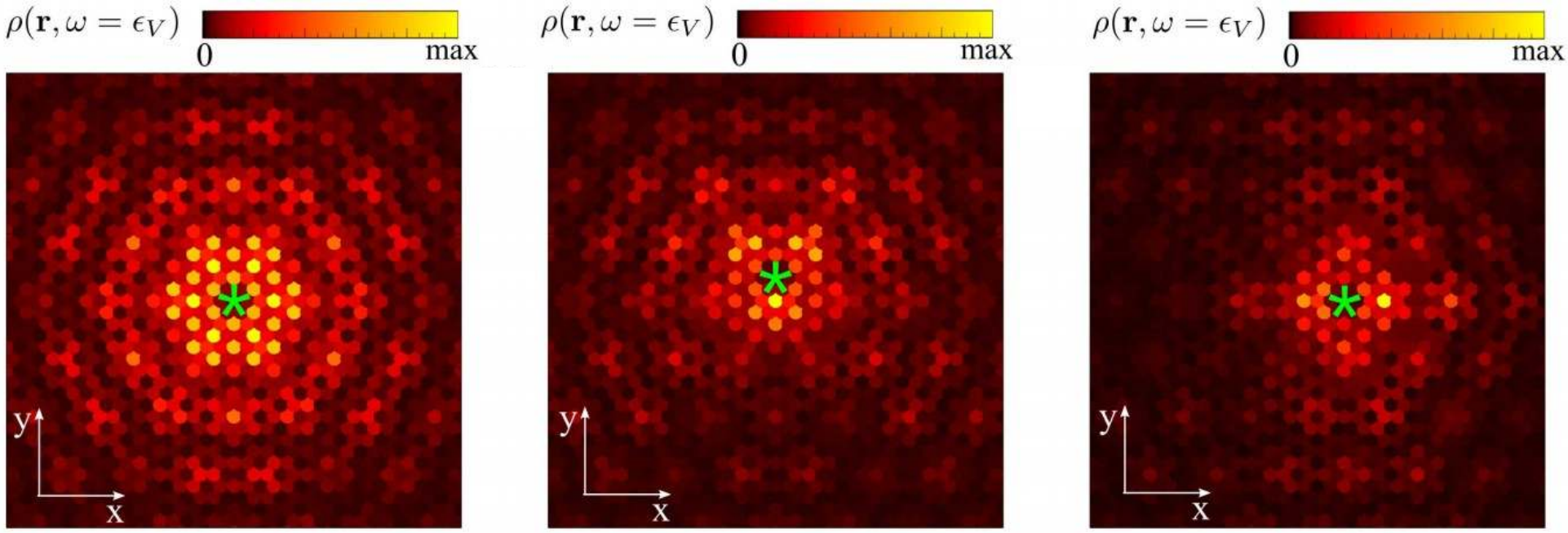

The YSR state wavefunction and the moire give rise to interference effects

Computing electronic properties

Quantum Lattice: A user interface to compute electronic properties

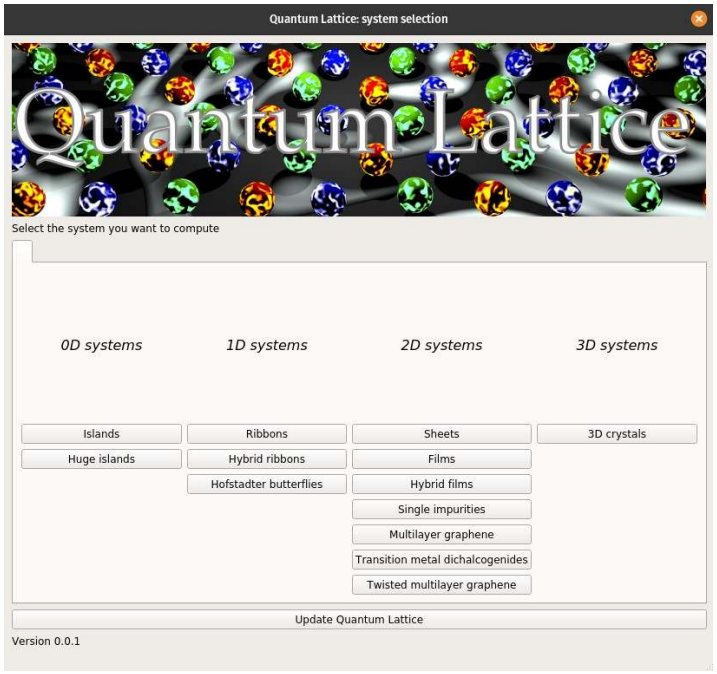

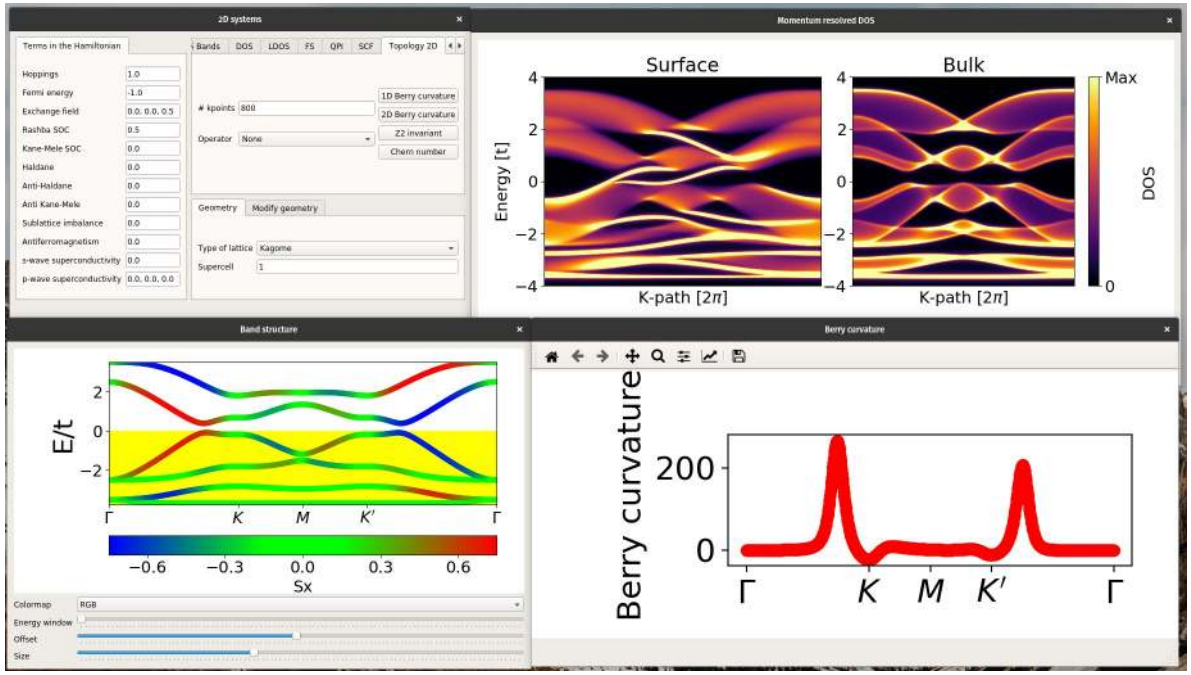

Quantum Lattice: open source interactive interface for tight binding modeling

https://github.com/joselado/quantum-lattice

Quantum matter in van der Waals materials school

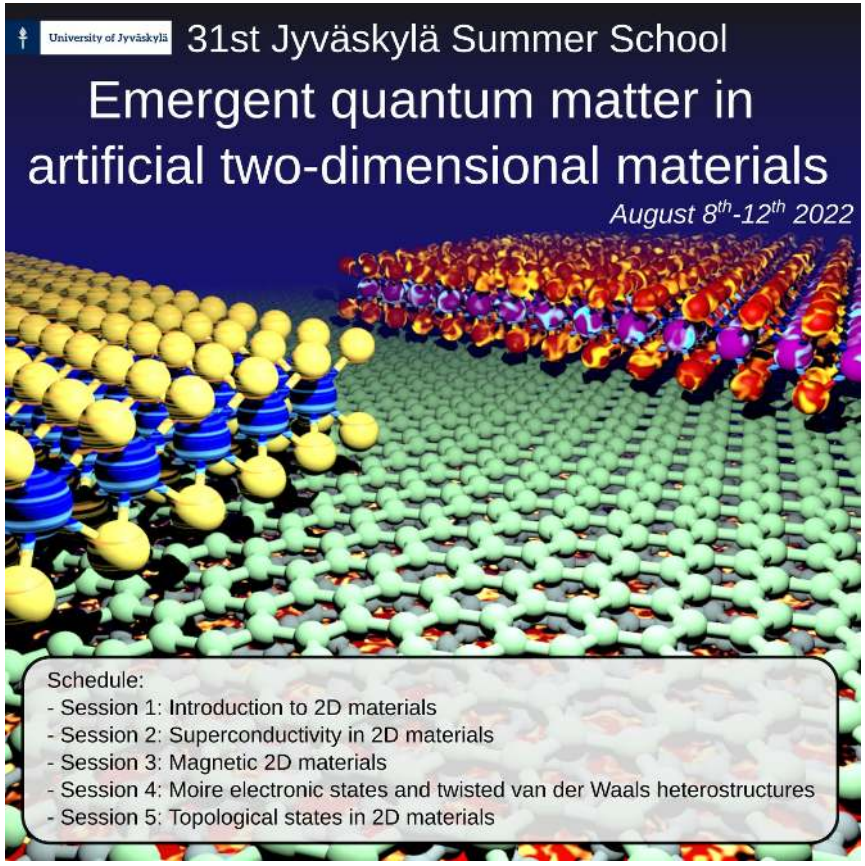

Recordings available at

https://www.youtube.com/channel/UCgnB-4CcqRQnvTi7P0cUakQ

- Session 1: Introduction to 2D materials
- Session 2: Superconductivity in 2D materials
- Session 3: Magnetic 2D materials
- Session 4: Moire electronic states and twisted van der Waals heterostructures
- Session 5: Topological states in 2D materials

Take home

Impurities in twisted moire systems can have strong impacts in the low energy dispersion, substantially modifying topological and correlated states

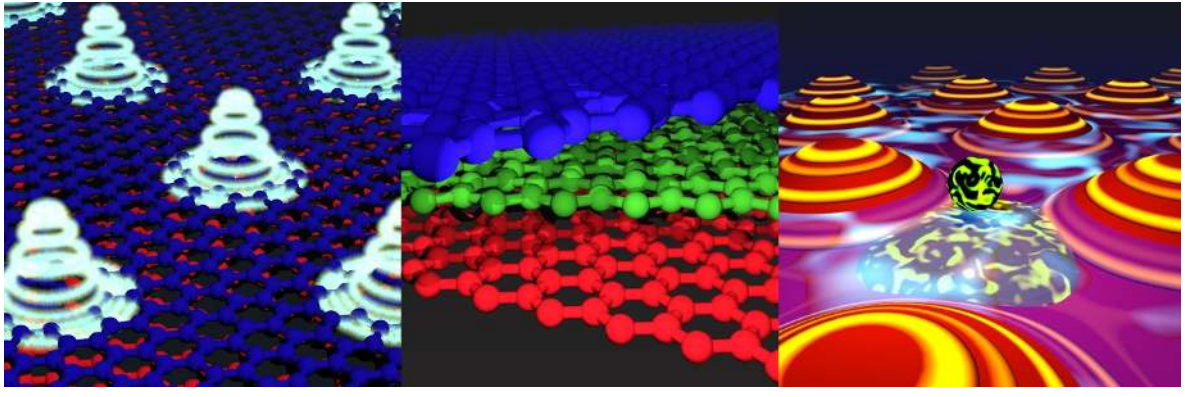

Phys. Rev. B 99, 245118 (2019)
Phys. Rev. Materials 3, 084003 (2019)
Phys. Rev. Research 2, 033357 (2020)
Phys. Rev. Materials 6, 094010 (2022)

Thank you!

Funding from

JANE AND AATOS ERKKO FOUNDATION

SUOMEN AKATEMIA